

# HANBURY-BROWN/TWISS INTERFEROMETRY FOR RELATIVISTIC HEAVY-ION COLLISIONS: THEORETICAL ASPECTS

Ulrich Heinz<sup>1</sup>

Institut für Theoretische Physik, Universität Regensburg,  
D-93040 Regensburg, Germany<sup>2</sup>

## 1. INTRODUCTION

Relativistic heavy-ion collisions at center of mass energies in the range of many to many hundreds of GeV per nucleon are performed with the ultimate goal of generating a new state of matter, the quark-gluon plasma (QGP). To make a QGP, one must heat and compress nuclear matter to such high energy densities that the hadrons overlap, creating a homogeneous piece of matter consisting only of the stuff usually hidden inside hadrons. In the region thus created the quarks and gluons, which are usually imprisoned inside the hadrons, become “deconfined”, i.e. they are able to travel around freely over regions which are large compared to the usual confinement length scale of about 1 fm (the typical radius of a hadron). Such matter existed in and filled all of the volume of the Early Universe during the first microsecond of its life but, as far as we know, it has not been recreated in the laboratory anywhere since.

How do we know our heavy-ion collision experiment has been successful in creating QGP? The answer to this question is surprisingly complex. The main reason for this is that quarks and gluons cannot travel over large distances outside the hot and dense QGP region and thus cannot be detected directly. Everything we can measure in the experiment provides therefore only indirect knowledge about the hoped-for QGP state. This is in particular true for the bulk of secondary particles produced in the collision which are hadrons: they can only be formed towards the end of the collision process when the reaction zone, by expansion into the surrounding vacuum, has cooled down sufficiently to allow the quarks and gluons to re-hadronize.

One approach to “prove” the making of QGP (which I stress must still be complemented by other experimental tests to check for consistency, see Jürgen Schukraft’s lectures [ 1] for examples) tries to reach a complete understanding of the space-time structure and dynamical state of the reaction zone at the “freeze-out point” where the measured hadrons decouple. One hopes and by now, from the experiments performed at the Brookhaven AGS and CERN SPS during the last decade, has accumulated a reasonably convincing body of evidence that at decoupling the matter has reached a

---

<sup>1</sup>Work supported by BMBF, DFG and GSI.

<sup>2</sup>Email: Ulrich.Heinz@physik.uni-regensburg.de

state of local thermal and perhaps even chemical equilibrium. It also features strong longitudinal and transverse collective (hydrodynamic) expansion. While some of the longitudinal expansion may be “primordial”, i.e. due to incomplete stopping of the two nuclei in the collision region, all of the transverse expansion must have been generated dynamically in the reaction. If it is possible to determine the energy density of the state at decoupling and simultaneously its expansion velocity, then one can try to extrapolate this state backwards in time to a point of vanishing transverse expansion and check whether there the energy density was above the critical value of about 1 GeV/fm<sup>3</sup> where one expects the phase transition to the QGP to occur.

But how does one measure the energy density at decoupling? To measure the total energy of the state is not too difficult: one measures the momenta of all emitted particles and their masses and adds them up. But to compute the energy density we must also know the volume of the reaction zone. And there is no known way to measure this volume directly. The collision fireball just doesn’t hang around long enough so that we could shine light on it (or a suitable other species of particles) and measure its size by diffraction.

The only known way to obtain indirect experimental information on the space-time structure of the particle emitting source created in a relativistic nuclear collision is through two-particle intensity (Hanbury-Brown–Twiss (HBT)) interferometry [ 2]. The goal of this method is to extract the *space-time* structure of the source from *momentum spectra* which are the only measurable quantities, making use of the quantum statistical correlations between pairs of identical particles. The basic idea, presented in a very naive and oversimplified way which to correct I will spend three hours of lectures during this Advanced Summer Institute, is as follows: Consider a source (for simplicity spherically symmetric) with radius  $R$ , and the emission of a pair of identical particles from point  $\mathbf{x}_1$  in the source with momentum  $\mathbf{p}_1$  and point  $\mathbf{x}_2$  with momentum  $\mathbf{p}_2$ . If these two points are well separated in phase-space, i.e. they satisfy

$$(x_1^i - x_2^i)(p_1^i - p_2^i) \gg 2\pi\hbar, \quad i = 1 \text{ or } i = 2 \text{ or } i = 3, \quad (1)$$

this process can be treated classically. If on the other hand,

$$(x_1^i - x_2^i)(p_1^i - p_2^i) \leq 2\pi\hbar, \quad i = 1, 2 \text{ and } 3, \quad (2)$$

the two particles sit close in phase-space, and quantum mechanics can no longer be ignored. The most important quantum mechanical correction to be taken into account is the (anti-)symmetrization of the two-particle wave function: it ensures vanishing probability for two identical fermions to originate from the same phase-space point, and for bosons it leads to an enhanced probability to find them at the same point in phase-space compared to the classical expectation (bosons are “social subjects”).

Since the distance in coordinate space ( $x_1^i - x_2^i$ ) is limited by the finite diameter  $2R$  of the source, we can force the system into the quantum domain by measuring particle pairs with smaller and smaller relative momentum  $\mathbf{p}_1 - \mathbf{p}_2$ . Once  $q_i \equiv p_1^i - p_2^i$  becomes smaller than  $\pi\hbar/R$ , the two particles can no longer avoid quantum mechanics by escaping to larger relative distances in coordinate space. Their emission probability will be affected by wave function symmetrization, leading in the case of bosons (fermions) to an enhanced (reduced) pair emission probability compared to the classical expectation (which would be simply the product of the individual single-particle emission probabilities). The two-particle *correlation function* is thus expected to begin to appreciably deviate from unity for relative momenta  $q < q^* \simeq (\hbar/R)$ . The critical value  $q^*$  at which this effect sets in (conveniently one chooses for  $q^*$  the value where the correlation is half

way between its maximum (minimum) value and 1) is thus a measure for the geometric radius  $R$  of the source.

So far the naive picture of how two-particle HBT interferometry works. Unfortunately, the only situation where it applies more or less directly is for photon interferometry of stars for which the method was invented. I will spend my time here in Dronen to explain to you why this naive picture is generically *wrong* and how to substitute it correctly. The basic reason why the above simple cartoon ceases to work in high energy nuclear and particle physics is that the sources created in hadronic or heavy-ion collisions live only for very short time periods and feature inhomogeneous temperature profiles and strong collective dynamical expansion. I will show you that for such sources the HBT radius parameters (half widths of the correlation function) generally don't measure the full source size, but only so-called "space-time regions of homogeneity" inside which the momentum distribution varies sufficiently little so that the particles can actually show the quantum statistical correlations. They also mix the spatial and temporal structure of the source, and we will learn tricks (in particular a new way of parametrizing the correlation functions) which are designed to unfold these different aspects from the data.

The size of the just mentioned homogeneity regions varies with the momentum of the emitted particles, causing an important dependence of the HBT parameters on the pair momentum. I will show you how this momentum dependence can be used to extract the strength of the collective flow of the source at decoupling. To do so in a quantitative way requires the detailed consideration of many physical features of the particle emission process. One such feature which I will discuss here in some detail is the fact that often some of the particles one uses in constructing the pair-correlation function don't come directly from the source but are created well after decoupling by the decay of unstable resonances. Resonance decays not only affect the size and momentum dependence of some of the HBT radius parameters but also the overall strength of the correlation as described by the so-called "chaoticity parameter"  $\lambda$ .

My lectures are structured in the following way: In the First Lecture, I discuss the general connection of the measured one- and two-particle spectra with the phase-space distribution of particles in the source. In particular I discuss the important aspects of "chaotic" versus "coherent" particle emission and how to implement them in a formal way. This establishes the formal background which I exploit in the Second Lecture to extract in a more quantitative way general ("model-independent") analytic relationships between the geometric and dynamic space-time structure of the source and certain features of the pair correlation function. In the Third Lecture I analyze these relationships quantitatively in the framework of a general class of model sources with finite geometric extension and three-dimensional collective expansion. The results should give you a good qualitative and even semi-quantitative feeling of the expected behaviour of the pair correlation function in relativistic heavy-ion collisions.

The Fourth Lecture should have presented a comparison of the calculations with the data, but fortunately the organizers gave me only three hours time so that I was spared the embarrassment of having to admit that at the present moment no quantitative such comparison exists: the theoretical analysis is still so new that most of the diagrams you will see are less than a few months old, and the new high-quality heavy-ion data which allow for the detailed multidimensional analysis advocated here are still so hot ("preliminary") that the experimentalists wouldn't give me permission to show them anyhow. Please look into Barbara Jacak's lecture notes in this volume [ 3] and into the Proceedings of the *Quark Matter '96* Conference in Heidelberg, 20-24 May 1996, if you want to catch a first glimpse of the data.

## 2. LECTURE 1: SPECTRA AND EMISSION FUNCTION

### 2.1. One- and two-particle spectra

The covariant single- and two-particle distributions are defined by

$$P_1(\mathbf{p}) = E \frac{dN}{d^3p} = E \langle \hat{a}_{\mathbf{p}}^+ \hat{a}_{\mathbf{p}} \rangle, \quad (3)$$

$$P_2(\mathbf{p}_a, \mathbf{p}_b) = E_a E_b \frac{dN}{d^3p_a d^3p_b} = E_a E_b \langle \hat{a}_{\mathbf{p}_a}^+ \hat{a}_{\mathbf{p}_b}^+ \hat{a}_{\mathbf{p}_b} \hat{a}_{\mathbf{p}_a} \rangle, \quad (4)$$

where  $\hat{a}_{\mathbf{p}}^+$  ( $\hat{a}_{\mathbf{p}}$ ) creates (destroys) a particle with momentum  $\mathbf{p}$ . The angular brackets denote an ensemble average,

$$\langle \hat{O} \rangle = \text{tr}(\hat{\rho} \hat{O}), \quad (5)$$

where  $\hat{\rho}$  is the density operator associated with the ensemble. (When talking about an ensemble we may think of either a single large, thermalized source, or a large number of similar, but not necessarily thermalized collision events.) The single-particle spectrum is normalized to the average number of particles,  $\langle N \rangle$ , per collision,

$$\int \frac{d^3p}{E} P_1(\mathbf{p}) = \langle N \rangle, \quad (6)$$

while the two-particle distribution is normalized to the number of possible pairs,  $\langle N(N-1) \rangle$ , per event:

$$\int \frac{d^3p_a}{E_a} \frac{d^3p_b}{E_b} P_2(\mathbf{p}_a, \mathbf{p}_b) = \langle N(N-1) \rangle. \quad (7)$$

The two-particle correlation function is defined as [ 5]

$$C(\mathbf{p}_a, \mathbf{p}_b) = \frac{\langle N \rangle^2}{\langle N(N-1) \rangle} \frac{P_2(\mathbf{p}_a, \mathbf{p}_b)}{P_1(\mathbf{p}_a) P_1(\mathbf{p}_b)}. \quad (8)$$

If the two particles are emitted independently and final state interactions are neglected I will show that it is possible to prove a generalized Wick theorem,

$$P_2(\mathbf{p}_a, \mathbf{p}_b) = \frac{\langle N(N-1) \rangle}{\langle N \rangle^2} \left( P_1(\mathbf{p}_a) P_1(\mathbf{p}_b) \pm |\bar{S}(\mathbf{p}_a, \mathbf{p}_b)|^2 \right), \quad (9)$$

where the plus (minus) sign refers to bosons (fermions), and we have defined the following covariant quantity:

$$\bar{S}(\mathbf{p}_a, \mathbf{p}_b) = \sqrt{E_a E_b} \langle \hat{a}_{\mathbf{p}_a}^+ \hat{a}_{\mathbf{p}_b} \rangle. \quad (10)$$

If the ensemble corresponds to a thermalized source in global thermodynamic equilibrium, i.e.  $\hat{\rho}$  is the (grand) canonical density operator, this is just the well-known “thermal Wick theorem” [ 6]. But even in nonthermal sources emission may be “chaotic”, i.e. the emission of particle  $a$  at point  $x_a$  may be completely independent from the emission of particle  $b$  at  $x_b$ . This can be described by assigning the wave function of the emitted particle a random phase  $\phi$  which is averaged over in the ensemble average. I will show that this is also sufficient to guarantee Wick’s theorem (10). – The opposite to independent, “chaotic” particle emission is emission from a coherent state (e.g. in a laser) where the phases of all emitted particles are fully correlated with each other; in

that case the second term in (10) is completely missing. The general situation can be parametrized by a superposition of density operators,

$$\hat{\rho} = \alpha \hat{\rho}_{\text{chaotic}} + (1 - \alpha) \hat{\rho}_{\text{coherent}}, \quad (11)$$

with  $0 \leq \alpha \leq 1$ , where only the chaotic first part contributes to the second term in (9):

$$\begin{aligned} \langle \hat{a}_a^+ \hat{a}_b^+ \hat{a}_b \hat{a}_a \rangle &= \langle \hat{a}_a^+ \hat{a}_a \rangle \langle \hat{a}_b^+ \hat{a}_b \rangle \pm \alpha |\langle \hat{a}_a^+ \hat{a}_b \rangle_{\text{ch}}|^2 \\ &+ \alpha(1 - \alpha) \left[ \left( \langle \hat{a}_a^+ \hat{a}_a \rangle_{\text{ch}} - \langle \hat{a}_a^+ \hat{a}_a \rangle_{\text{coh}} \right) \left( \langle \hat{a}_b^+ \hat{a}_b \rangle_{\text{ch}} - \langle \hat{a}_b^+ \hat{a}_b \rangle_{\text{coh}} \right) \right]. \end{aligned} \quad (12)$$

The last term contributes only if the chaotic and coherent parts of the density operator generate different single-particle spectra. One easily checks that for  $\alpha < 1$  in such an ensemble the correlations are “incomplete”, i.e. at  $\mathbf{p}_a = \mathbf{p}_b$  the correlation function (8) approaches a value less than 2 for bosons and larger than 0 for fermions. – Since so far the heavy ion data don’t appear to require a coherent component in the particle production process, I will for the remainder of these lectures assume  $\alpha = 1$  and refer the interested reader for the possible effects from partial coherence to the literature [7].

Assuming the generalized Wick theorem (9) the correlation function (8) can be written as

$$C(\mathbf{p}_a, \mathbf{p}_b) = 1 \pm \frac{|\langle \hat{a}_{\mathbf{p}_a}^+ \hat{a}_{\mathbf{p}_b} \rangle|^2}{\langle \hat{a}_{\mathbf{p}_a}^+ \hat{a}_{\mathbf{p}_a} \rangle \langle \hat{a}_{\mathbf{p}_b}^+ \hat{a}_{\mathbf{p}_b} \rangle}. \quad (13)$$

Note that the second term is positive definite, i.e. the correlation function cannot, for example, oscillate around unity. [If you see such a behaviour in the literature [8] (and the authors did not include final state interactions) it is wrong.]

From now on I will assume that the emitted particles are bosons, and for convenience I will call them pions, although nearly everything in the first two lectures applies equally well to other bosonic particles (except where explicitly stated). In the last Lecture I will be a little more specific and distinguish between 2-pion and 2-kaon correlations for comparison.

## 2.2. The generalized Wick theorem

Pions are created in heavy-ion collisions throughout the history of the collision process, but we are only interested in those pions which reach the detector as free, non-interacting particles. (Unfortunately, pion interferometry can only be practically performed with charged pions, because neutral pions decay too rapidly. But charged pions have a long-range final state interaction, the Coulomb repulsion from the other pion in the pair with equal charge, as well as the attractive or repulsive Coulomb interaction with the hundreds of other produced charged particles, including the charge of the protons in the fireball. A proper treatment of this many-body Coulomb problem is a difficult task [9]. Since I don’t know yet how to do it properly, I will simply neglect the Coulomb interaction in the final state – assuming that somehow the experimentalists know how to approximately correct their measured correlations for it [3].)

We assume that the last interaction of the pion, in which the finally observed pion is created in its free asymptotic state, can be parametrized by a classical source amplitude  $J(x)$ . The solution of the free Klein-Gordon equation for pions generated by such a classical current,

$$(\square + m^2)\hat{\phi}(x) = J(x), \quad (14)$$

with outgoing boundary conditions is given [5] by a classical (“coherent”) state

$$|J\rangle = e^{-\bar{n}/2} \exp\left(i \int d^3p \tilde{J}(\mathbf{p}) \hat{a}_{\mathbf{p}}^+\right) |0\rangle \quad (15)$$

where

$$\tilde{J}(\mathbf{p}) = \int \frac{d^4x}{\sqrt{(2\pi)^3 2E_p}} \exp[i(E_p t - \mathbf{p} \cdot \mathbf{x})] J(x) \quad (16)$$

is the on-shell Fourier transform of the source  $J(x)$ , and the normalization of the state is given by

$$\bar{n} = \int d^3p |\tilde{J}(\mathbf{p})|^2. \quad (17)$$

The state (15) is an eigenstate of the destruction operator:

$$\hat{a}_{\mathbf{p}}|J\rangle = i\tilde{J}(\mathbf{p})|J\rangle. \quad (18)$$

### 2.2.1. Emission from a single coherent state

If there is only a single classical source  $J(x)$ , the corresponding density operator of the “ensemble” is just the projection operator on the coherent state,  $\hat{\rho}_{\text{coherent}} = |J\rangle\langle J|$ , and, using (18), the single- and two-particle spectra (3,4) are easily evaluated:

$$E \frac{dN}{d^3p} = E \langle J | \hat{a}_{\mathbf{p}}^+ \hat{a}_{\mathbf{p}} | J \rangle = E |\tilde{J}(\mathbf{p})|^2, \quad (19)$$

$$E_a E_b \frac{dN}{d^3p_a d^3p_b} = E_a E_b \langle J | \hat{a}_{\mathbf{p}_a}^+ \hat{a}_{\mathbf{p}_b}^+ \hat{a}_{\mathbf{p}_b} \hat{a}_{\mathbf{p}_a} | J \rangle = E_a |\tilde{J}(\mathbf{p}_a)|^2 \cdot E_b |\tilde{J}(\mathbf{p}_b)|^2. \quad (20)$$

Obviously, there is no exchange term in the two-particle spectrum which is simply given by the product of the single-particle spectra. *A coherent state thus has no Bose-Einstein correlations.*

### 2.2.2. Emission by a chaotic superposition of classical sources

This changes if we consider a superposition of classical source amplitudes each of which emits free pions independently, i.e. with a random phase [ 5]:

$$J(x) = \sum_{i=1}^N e^{i\phi_i} e^{-ip_i \cdot (x-x_i)} J_0(x-x_i). \quad (21)$$

The construction rule [ 10, 11] for this source is obvious: we take  $N$  sources  $J_0(x)$  with identical internal structure, give each of them a boost with 4-momentum  $p_i$ , then translate them to different positions  $x_i$  in the fireball and supply them with a random phase  $\phi_i$ . This allows for arbitrary  $x$ - $p$  correlations [ 10] (i.e. correlations between the momentum spectrum of the emitted particles and the point from where they are emitted). The momenta  $p_i$  of the sources can, but need not be on the pion mass-shell; for example, the source could be a decaying  $\Delta$ -resonance with 3-momentum  $\mathbf{p}_i$ . The on-shell Fourier transform of (21) is

$$\tilde{J}(\mathbf{p}) = \sum_{i=1}^N e^{i\phi_i} e^{ip \cdot x_i} \tilde{J}_0(p-p_i), \quad (22)$$

where

$$\tilde{J}_0(p-p_i) = \int \frac{d^4x}{\sqrt{(2\pi)^3 2E_p}} e^{i(p-p_i) \cdot x} J_0(x) \quad (23)$$

is the (regular) Fourier transform of  $J_0(x)$ , and  $p$  is on-shell while  $p_i$  may be off-shell. The state  $|J\rangle$  which is defined by inserting (22) into (15) now depends on the parameters  $\{x_i, p_i, \phi_i; i = 1, \dots, N\}$ :

$$|J\rangle \equiv |J[N; \{x, p, \phi\}]\rangle. \quad (24)$$

The ensemble of sources can be defined in terms of a density operator  $\hat{\rho}$  which fixes the distribution of these parameters. We assume that the number of sources  $N$  is distributed with a probability distribution  $P_N$ , the phases  $\phi$  are distributed randomly between 0 and  $2\pi$ , and the source positions  $x_i$  and momenta  $p_i$  are distributed with a phase-space density  $\rho(x, p)$ , with normalizations

$$\sum_{N=0}^{\infty} P_N = 1, \quad \sum_{N=0}^{\infty} N P_N = \langle N \rangle, \quad \int d^4x d^4p \rho(x, p) = 1. \quad (25)$$

The corresponding ensemble average is given by

$$\text{tr}(\hat{\rho} \hat{O}) = \sum_{N=0}^{\infty} P_N \prod_{i=1}^N \int d^4x_i d^4p_i \rho(x_i, p_i) \int_0^{2\pi} \frac{d\phi_i}{2\pi} \langle J[N; \{x, p, \phi\}] | \hat{O} | J[N; \{x, p, \phi\}] \rangle. \quad (26)$$

The calculation of the single-particle spectrum is straightforward:

$$\begin{aligned} \langle \hat{a}_{\mathbf{p}}^+ \hat{a}_{\mathbf{p}} \rangle &= \sum_{N=0}^{\infty} P_N \prod_{i=1}^N \int d^4x_i d^4p_i \rho(x_i, p_i) \int_0^{2\pi} \frac{d\phi_i}{2\pi} \\ &\times \sum_{n, n'=1}^N e^{i(\phi_n - \phi_{n'})} e^{ip \cdot (x_n - x_{n'})} \tilde{J}_0^*(p - p_{n'}) \tilde{J}_0(p - p_n). \end{aligned} \quad (27)$$

After performing the integrations over the phases  $\phi_i$  in the double sum over  $n$  and  $n'$ , only the diagonal terms with  $n=n'$  survive. For each term in the remaining single sum over  $n$  the integrations over  $x_i$  and  $p_i$ ,  $i \neq n$ , can be done using the normalization condition (25). After suitably relabelling the dummy integration variables for the one remaining  $x$ - and  $p$ -integration we end up with  $N$  identical terms under the sum over  $n$ . This allows to perform the sum over  $N$ , and we simply get

$$P_1(\mathbf{p}) = E_p \langle |\tilde{J}(\mathbf{p})|^2 \rangle = \langle N \rangle E_p \int d^4x' d^4p' \rho(x', p') |\tilde{J}_0(p - p')|^2 \quad (28)$$

$$= \langle N \rangle E_p \int d^4p' \tilde{\rho}(p') |\tilde{J}_0(p - p')|^2. \quad (29)$$

The single particle spectrum is thus obtained by folding the intrinsic momentum spectrum  $|\tilde{J}_0(p)|^2$  of the individual source currents  $J_0$  with the 4-momentum distribution of the sources,  $\tilde{\rho}(p) = \int d^4x \rho(x, p)$ .

The algebra for the two-particle spectrum is a little more involved. It is useful to first compute

$$\begin{aligned} \langle \hat{a}_{\mathbf{p}_a}^+ \hat{a}_{\mathbf{p}_b} \rangle &= \sum_{N=0}^{\infty} P_N \prod_{i=1}^N \int d^4x_i d^4p_i \rho(x_i, p_i) \int_0^{2\pi} \frac{d\phi_i}{2\pi} \\ &\times \sum_{n, n'=1}^N e^{i(\phi_n - \phi_{n'})} e^{i(p_b \cdot x_n - p_a \cdot x_{n'})} \tilde{J}_0^*(p_a - p_{n'}) \tilde{J}_0(p_b - p_n). \end{aligned} \quad (30)$$

Again only the terms  $n=n'$  survive the phase average, and after doing the dummy integrations over  $x_i, p_i$ ,  $i \neq n$ , one finds that the remaining sum over  $n$  contains again  $N$  identical terms, such that the sum over  $N$  can be performed:

$$\langle \hat{a}_{\mathbf{p}_a}^+ \hat{a}_{\mathbf{p}_b} \rangle = \langle N \rangle \int d^4x' d^4p' \rho(x', p') e^{i(p_b - p_a) \cdot x'} \tilde{J}_0^*(p_a - p') \tilde{J}_0(p_b - p'). \quad (31)$$

With this auxiliary result at hand we can now attack the two-particle spectrum. From the definitions one finds

$$\begin{aligned} \langle \hat{a}_{\mathbf{p}_a}^+ \hat{a}_{\mathbf{p}_b}^+ \hat{a}_{\mathbf{p}_b} \hat{a}_{\mathbf{p}_a} \rangle &= \sum_{N=0}^{\infty} P_N \prod_{i=1}^N \int d^4 x_i d^4 p_i \rho(x_i, p_i) \int_0^{2\pi} \frac{d\phi_i}{2\pi} \\ &\times \sum_{n, n', m, m'=1}^N e^{i(\phi_n + \phi_m - \phi_{n'} - \phi_{m'})} e^{ip_a \cdot (x_n - x_{n'})} e^{ip_b \cdot (x_m - x_{m'})} \\ &\times \tilde{J}_0^*(p_a - p_{n'}) \tilde{J}_0^*(p_b - p_{m'}) \tilde{J}_0(p_b - p_m) \tilde{J}_0(p_a - p_n). \end{aligned} \quad (32)$$

The integration over the phases  $\phi_i$  now yields two types of nonvanishing contributions:  $n = n', m = m'$  and  $n = m', m = n'$ . The term where all four summation indices are equal,  $n = m = n' = m'$ , should be omitted [ 5]: it corresponds to emission of both particles from the same elementary source, and if one carefully first puts the whole system in a finite volume  $V$ , performs the calculation there and lets  $V \rightarrow \infty$  in the end, then this term is suppressed relative to the others by a factor  $1/V$ . We thus get

$$\begin{aligned} \langle \hat{a}_{\mathbf{p}_a}^+ \hat{a}_{\mathbf{p}_b}^+ \hat{a}_{\mathbf{p}_b} \hat{a}_{\mathbf{p}_a} \rangle &= \sum_{N=0}^{\infty} P_N \prod_{i=1}^N \int d^4 x_i d^4 p_i \rho(x_i, p_i) \sum_{n \neq m}^N \left[ |\tilde{J}_0(p_a - p_n)|^2 |\tilde{J}_0(p_b - p_m)|^2 \right. \\ &+ \left. e^{i(p_a - p_b) \cdot (x_n - x_m)} \tilde{J}_0^*(p_a - p_m) \tilde{J}_0^*(p_b - p_n) \tilde{J}_0(p_b - p_m) \tilde{J}_0(p_a - p_n) \right] \\ &= \sum_{N=0}^{\infty} P_N \prod_{i=1}^N \int d^4 x_i d^4 p_i \rho(x_i, p_i) \\ &\times \left[ \left( \sum_{n \neq m}^N |\tilde{J}_0(p_a - p_n)|^2 \right) \left( \sum_{m=1}^N |\tilde{J}_0(p_b - p_m)|^2 \right) \right. \\ &+ \left( \sum_{n \neq m}^N e^{i(p_a - p_b) \cdot x_n} \tilde{J}_0^*(p_b - p_n) \tilde{J}_0(p_a - p_n) \right) \\ &\times \left. \left( \sum_{m=1}^N e^{-i(p_a - p_b) \cdot x_m} \tilde{J}_0(p_b - p_m) \tilde{J}_0^*(p_a - p_m) \right) \right]. \end{aligned} \quad (33)$$

After again doing the dummy integrations over  $x_i, p_i$ ,  $i \neq n, m$ , one realizes that each of the two terms in the square bracket contains  $N(N-1)$  identical terms, yielding a factor  $\langle N(N-1) \rangle$  after performing the sum over  $N$ . Up to this factor, the first term is just a product of two terms of the type (28), i.e. a product of single-particle spectra, while the second term is recognized as a product of (31) and its complex conjugate. We thus have

$$P_2(\mathbf{p}_a, \mathbf{p}_b) = \frac{\langle N(N-1) \rangle}{\langle N \rangle^2} E_a E_b \left[ \langle \hat{a}_{\mathbf{p}_a}^+ \hat{a}_{\mathbf{p}_a} \rangle \langle \hat{a}_{\mathbf{p}_b}^+ \hat{a}_{\mathbf{p}_b} \rangle + |\langle \hat{a}_{\mathbf{p}_a}^+ \hat{a}_{\mathbf{p}_b} \rangle|^2 \right] \quad (34)$$

$$= \frac{\langle N(N-1) \rangle}{\langle N \rangle^2} E_a E_b \left[ \langle |\tilde{J}(\mathbf{p}_a)|^2 \rangle \langle |\tilde{J}(\mathbf{p}_b)|^2 \rangle + |\langle \tilde{J}^*(\mathbf{p}_a) \tilde{J}(\mathbf{p}_b) \rangle|^2 \right], \quad (35)$$

which proves the generalized Wick theorem (9).

### 2.3. Source Wigner function and spectra

These expressions can be rewritten in a very nice and suggestive way by introducing the so-called ‘‘emission function’’  $S(x, K)$  [ 12, 13, 7]:

$$S(x, K) = \int \frac{d^4 y}{2(2\pi)^3} e^{-iK \cdot y} \left\langle J^*(x + \frac{1}{2}y) J(x - \frac{1}{2}y) \right\rangle. \quad (36)$$

It is the Wigner transform of the density matrix associated with the classical source amplitudes  $J(x)$ . This Wigner density is a quantum mechanical object defined in phase-space  $(x, K)$ ; in general it is neither positive definite nor real. But, when integrated over  $x$  or  $K$  it yields the classical (positive definite and real) source density in momentum or coordinate space, respectively, in exactly the same way as a classical phase-space density would behave. Furthermore, textbooks on Wigner functions show that their non-reality and non-positivity are genuine quantum effects resulting from the uncertainty relation and are concentrated at short phase-space distances; when the Wigner function is averaged over phase-space volumes which are large compared to the volume  $(2\pi\hbar)^3$  of an elementary phase-space cell, the result is real and positive definite and behaves exactly like a classical phase-space density.

The emission function  $S(x, K)$  is thus the quantum mechanical analogue of the classical phase-space distribution which gives the probability of finding at point  $x$  a source which emits free pions with momentum  $K$ . Please note that  $K$  in  $S(x, K)$  can be off-shell. Also, it is defined in terms of a 4-dimensional Wigner transform of the source density matrix [ 12], in contrast to the 3-dimensional expression suggested by Pratt [ 13] which neglects retardation and off-shell effects.

Using Eq. (16) it is easy to establish the following relationship:

$$\begin{aligned}\tilde{J}^*(\mathbf{p}_a) \tilde{J}(\mathbf{p}_b) &= \int \frac{d^4x_1 d^4x_2}{(2\pi)^3 2\sqrt{E_a E_b}} \exp(-ip_a \cdot x_1 + ip_b \cdot x_2) J^*(x_1) J(x_2) \\ &= \int \frac{d^4x d^4y}{(2\pi)^3 2\sqrt{E_a E_b}} \exp(-iq \cdot x - iK \cdot y) J^*(x + \frac{1}{2}y) J(x - \frac{1}{2}y),\end{aligned}\quad (37)$$

where  $x = \frac{1}{2}(x_1 x_2)$  and  $y = x_1 - x_2$ . Inserting this into Eqs. (28) and (35) one finds the fundamental relations:

$$E_K \frac{dN}{d^3K} = \int d^4x S(x, K), \quad (38)$$

$$C(\mathbf{q}, \mathbf{K}) = 1 + \frac{|\int d^4x S(x, K) e^{iq \cdot x}|^2}{\int d^4x S(x, K + \frac{1}{2}q) \int d^4x S(x, K - \frac{1}{2}q)}. \quad (39)$$

For the single-particle spectrum (38), the Wigner function  $S(x, K)$  on the r.h.s. must be evaluated on-shell, i.e. at  $K^0 = E_K = \sqrt{m^2 + \mathbf{K}^2}$ . For the correlator (39) we have defined the relative momentum  $\mathbf{q} = \mathbf{p}_a - \mathbf{p}_b$ ,  $q^0 = E_a - E_b$  between the two particles in the pair, and the total momentum of the pair  $\mathbf{K} = (\mathbf{p}_a + \mathbf{p}_b)/2$ ,  $K^0 = (E_a + E_b)/2$ . Of course, since the 4-momenta  $p_{a,b}$  of the two measured particles are on-shell,  $p_i^0 = E_i = \sqrt{m^2 + \mathbf{p}_i^2}$ , the 4-momenta  $q$  and  $K$  are in general off-shell. They satisfy the orthogonality relation

$$q \cdot K = 0. \quad (40)$$

Thus, the Wigner function on the r.h.s. of Eq. (39) is *not* evaluated at the on-shell point  $K^0 = E_K$ . This implies that for the correlator, in principle, we need to know the off-shell behaviour of the emission function, i.e. the quantum mechanical structure of the source. Obviously, this makes the problem appear rather untractable!

Fortunately, nature is nice to us: the interesting behaviour of the correlator (its deviation from unity) is concentrated at small values of  $|\mathbf{q}|$ . Expanding  $K^0 = (E_a + E_b)/2$  for small  $q$  one finds

$$K^0 = E_K \left( 1 + \frac{\mathbf{q}^2}{8E_K^2} + \mathcal{O}\left(\frac{\mathbf{q}^4}{E_K^4}\right) \right) \approx E_K. \quad (41)$$

Since the relevant range of  $q$  is given by the inverse size of the source (more properly: the inverse size of the regions of homogeneity in the source – see Lecture 2), the validity of this approximation is ensured in practice as long as the Compton wavelength of the particles is small compared to this “source size”. For the case of pion, kaon, or proton interferometry for heavy-ion collisions this is true automatically due to the rest mass of the particles: even for pions at rest, the Compton wavelength of 1.4 fm is comfortably smaller than any typical nuclear source size. This is of enormous practical importance because it allows you essentially to replace the source Wigner density by a classical phase-space distribution function for on-shell particles. This provides a necessary theoretical foundation for the calculation of HBT correlations from classical hydrodynamic or kinetic (e.g. cascade or molecular dynamics) simulations of the collision.

In photon interferometry there is no rest mass available to help you: for photons, the approximation  $K^0 \approx E_K$  can only be justified if they escape from the source with high momentum, and in HBT interferometry with soft photons the quantum mechanical nature of the emission function needs to be explicitly considered. In practice this means that one must study the photon production processes microscopically and quantum mechanically.

If the single-particle spectrum is an exponential function of the energy then it is easy to prove [ 14] that one can replace the product of single-particle distributions in the denominator of (39) by the square of the single-particle spectrum evaluated at the average momentum  $K$ :

$$C(\mathbf{q}, \mathbf{K}) \approx 1 + \left| \frac{\int d^4x e^{iq \cdot x} S(x, K)}{\int d^4x S(x, K)} \right|^2 \equiv 1 + \left| \langle e^{iq \cdot x} \rangle \right|^2. \quad (42)$$

The deviations from this approximation are proportional to the curvature of the single-particle distribution in logarithmic representation [ 14]. They are small in practice because the measured single-particle spectra are usually more or less exponential. In the second equality of (42) we defined  $\langle \dots \rangle$  as the average taken with the emission function; due to the  $K$ -dependence of  $S(x, K)$  this average is a function of  $K$ . This notation will be used extensively in Lecture 2.

The ensemble average on the r.h.s. of (36) is defined in the sense of Eq. (26) and can be evaluated with the help of the definition (21). One finds

$$S(x, K) = \langle N \rangle \int d^4z d^4q \rho(x - z, q) S_0(z, K - q), \quad (43)$$

where

$$S_0(x, p) = \int \frac{d^4y}{2(2\pi)^3} e^{-ip \cdot y} J_0^*(x + \frac{1}{2}y) J_0(x - \frac{1}{2}y) \quad (44)$$

is the Wigner function associated with an individual source  $J_0$ . This establishes a similar folding relation for the Wigner function itself as we have already obtained in (29) for the single-particle spectrum: the emission function of the complete source is obtained by folding the Wigner function for an individual pion source  $J_0$  with the Wigner distribution  $\rho$  of these sources. Eq. (43) is useful for the calculation of quantum statistical correlations from classical Monte Carlo event generators for heavy-ion collisions:  $\langle N \rangle \rho(x, p)$  can be considered as the distribution of the classical phase-space coordinates of the pion emitters (decaying resonances or 2-body collision systems), and  $S_0(x, p)$  as the Wigner function of the free pions emitted at these points (for example, a Gaussian in Quantum Molecular Dynamics calculations [ 15]). Replacing the former by a sum of  $\delta$ -functions describing the space-time locations of the last interactions and

the pion momenta just afterwards, and the latter by a product of two Gaussians with momentum spread  $\Delta p$  and coordinate spread  $\Delta x$  such that  $\Delta x \Delta p \geq \hbar/2$ , we recover the expressions derived in [16].

The fundamental relations (38) and (39) resp. (42) show that *both the single-particle spectrum and the two-particle correlation function can be expressed as simple integrals over the emission function*. The emission function thus is the crucial ingredient in the theory of HBT interferometry: if it is known, the calculation of one- and two-particle spectra is straightforward (even if the evaluation of the integrals may in some cases be technically involved); more interestingly, measurements of the one- and two-particle spectra provide access to the emission function and thus to the space-time structure of the source. This latter aspect is, of course, the motivation for exploiting HBT in practice. In my second and third Lecture I will concentrate on the question to what extent this access to the space-time structure from only momentum-space data really works, whether it is complete, and (since we will find it is not and HBT analyses will thus be necessarily model-dependent) what can be reliably said about the extension and dynamical space-time structure of the source anyhow, based on a minimal set of intuitive and highly suggestive model assumptions.

### 3. LECTURE 2: MODEL-INDEPENDENT DISCUSSION OF HBT CORRELATION FUNCTIONS

In this lecture I will discuss very general relations between the space-time structure of the source (as encoded in the  $x$ -dependence of the emission function  $S(x, K)$ ) and the shape of the two-particle correlation function. These relations are valid for arbitrary emission functions, and in this sense the discussion is *model-independent*. It nevertheless provides important insight into the physical features of HBT interferometry, in particular for short-lived dynamical sources, and it clarifies what HBT can achieve and what not.

#### 3.1. The mass-shell constraint

Expressions (39,42) show that the correlation function is related to the emission function by a Fourier transformation. At first sight this might suggest that one should easily be able to reconstruct the emission function from the measured correlation function by inverse Fourier transformation, the single particle spectrum (38) providing the normalization. This is, however, not correct. The reason is that, since the correlation function is constructed from the on-shell momenta of the measured particle pairs, not all four components of the relative momentum  $q$  occurring on the r.h.s. of (42) are independent. They are related by the “mass-shell constraint” (40) which can, for instance, be solved for  $q^0$ :

$$q^0 = \boldsymbol{\beta} \cdot \mathbf{q} \quad \text{with} \quad \boldsymbol{\beta} = \frac{\mathbf{K}}{K^0} \approx \frac{\mathbf{K}}{E_K}. \quad (45)$$

$\boldsymbol{\beta}$  is (approximately) the velocity of the c.m. of the particle pair. The Fourier transform in (42) is therefore not invertible, and the reconstruction of the space-time structure of the source from HBT measurements will thus always require additional model assumptions.

It is instructive to insert (45) into (42):

$$C(\mathbf{q}, \mathbf{K}) \approx 1 + \left| \frac{\int d^4x \exp(i\mathbf{q} \cdot (\mathbf{x} - \boldsymbol{\beta} t)) S(x, K)}{\int d^4x S(x, K)} \right|^2. \quad (46)$$

This shows that the correlator  $C(\mathbf{q}, \mathbf{K})$  actually mixes the spatial and temporal information on the source in a non-trivial way which depends on the pair velocity  $\beta$ . Only for time-independent sources things seem to be simple: the correlator then just measures the Fourier transform of the spatial source distribution. Closer inspection shows, however, that it does so only in the directions *perpendicular* to  $\beta$  since the time integration leads to a  $\delta$ -function  $\delta(\beta \cdot \mathbf{q})$ :

$$\lim_{T \rightarrow \infty} \left| \frac{\int_{-T}^T dt \exp(-i \mathbf{q} \cdot \beta t)}{\int_{-T}^T dt} \right|^2 = \lim_{T \rightarrow \infty} \frac{2\pi}{T} \delta(\mathbf{q} \cdot \beta). \quad (47)$$

This implies that there are no correlations in the direction *parallel* to the pair velocity  $\beta$  (which will be called the “outward” direction below), i.e.  $C = 1$  for  $q_{\text{out}} \neq 0$ . The width of the correlator in this direction vanishes! This should puzzle you: wouldn’t you have thought that the width of the correlator in the “outward” direction is inversely related to the source size in that direction (which is, of course, perfectly finite)? As we will see in the next subsection this unexpected behaviour is just another consequence of the mixing of the spatial and temporal structure of the source in the correlator: The width parameter of the correlator in the “outward” direction receives also a contribution from the lifetime of the source which in this case diverges, leading to the vanishing width of the correlator.

### 3.2. $K$ -dependence of the correlator

Eq. (42) shows that in general the correlator is a function of *both*  $\mathbf{q}$  and  $\mathbf{K}$ . Only if the emission function factorizes in  $x$  and  $K$ ,  $S(x, K) = F(x)G(K)$ , which means that every point  $x$  in the source emits particles with the same momentum spectrum  $G(K)$  (no “ $x$ - $K$ -correlations”), the  $K$ -dependence in  $G(K)$  cancels between numerator and denominator of (42), and the correlator seems to be  $K$ -independent. However, not even this is really true: even after the cancellation of the explicit  $K$ -dependence  $G(K)$ , there remains an implicit  $K$ -dependence via the pair velocity  $\beta \approx \mathbf{K}/E_K$  in the exponent on the r.h.s. of Eq. (46)! Only if both conditions, factorization of the emission function in  $x$  and  $K$  *and* time-independence of the source, apply simultaneously, the correlation function is truly  $K$ -independent (because then the  $\beta$ -dependence resides only in the  $\delta$ -function (47)).

The only practical situation which I know where this occurs and a  $K$ -independent correlation function should thus be expected is in HBT interferometry of stars for which the method was invented [17]. It is hard to believe that this complication in the application of the original HBT idea to high-energy collisions went nearly unnoticed for more than 20 years and was stumbled upon more or less empirically by Scott Pratt in his pioneering work on HBT interferometry for heavy-ion collisions [13] only in 1984!

If one parametrises it by a Gaussian in  $q$  (see below) this means that in general the parameters (“HBT radii”) depend on  $K$ . Typical sources of  $x$ - $K$  correlations in the emission function are a collective expansion of the emitter and/or temperature gradients in the particle source: in both cases the momentum spectrum  $\sim \exp[-p \cdot u(x)/T(x)]$  of the emitted particles (where  $u^\mu(x)$  is the 4-velocity of the expansion flow) depends on the emission point. In the case of collective expansion, the spectra from different emission points are Doppler shifted relative to each other. If there are temperature gradients, e.g. a high temperature in the center and cooler matter at the edges, the source will look smaller for high-momentum particles (which come mostly from the hot center) than for low-momentum ones (which receive larger contributions also from the cooler outward regions).

We thus see that collective expansion of the source induces a  $K$ -dependence of the correlation function. But so do temperature gradients. The crucial question is: does a careful measurement of the correlation function, in particular of its  $K$ -dependence, permit a separation of such effects, i.e. can the collective dynamics of the source be quantitatively determined through HBT experiments? We will see that this is not an easy task; however, with sufficiently good data, it should be possible. In any case, the  $K$ -dependence of the correlator is a decisive feature which puts the HBT game into a completely new ball park. Even if it sounds exaggerated and may at first offend some of my experimentalist friends who are busy fighting the limited statistics of their data: two-particle correlation measurements which are not able to resolve the  $K$ -dependence of the HBT parameters are, in high energy nuclear and particle physics, essentially useless. [Unfortunately, this applies to all the HBT data from  $pp$  and  $e^+e^-$  collisions which I am aware of. In my opinion, a renewed investigation of two-particle correlations from  $pp$  and  $e^+e^-$  collisions, using the powerful new tool of multidimensional HBT analysis, should be a high priority project – as it is, we have practically nothing with which to compare our heavy-ion results in a meaningful way.]

### 3.3. The Gaussian approximation

As motivated in the Introduction, the most interesting feature of the two-particle correlation function is its half-width. Actually, since the relative momentum  $\mathbf{q} = \mathbf{p}_1 - \mathbf{p}_2$  has three Cartesian components, the fall-off of the correlator for increasing  $q$  is not described by a single half-width, but rather by a (symmetric)  $3 \times 3$  tensor [ 18] which describes the curvature of the correlation function near  $\mathbf{q} = 0$ . We will see that in fact nearly all relevant information that can be extracted from the correlation function resides in the 6 independent components of this tensor [ 19]. This in turn implies that in order to compute the correlation function  $C$  it is sufficient to approximate the source function  $S$  by a Gaussian in  $x$  which contains only information on its space-time moments up to second order. [Gaussian approximations for the emission function have been used for the discussion of HBT correlation functions in many different variants [ 14, 18, 19, 20, 21, 22, 23, 24], a perfect example how research proceeds by trial and error. Here I give the rigorous derivation first published in [ 23].]

Let us write the arbitrary emission function  $S(x, K)$  in the following form:

$$S(x, K) = N(K) S(\bar{x}(K), K) e^{-\frac{1}{2} \tilde{x}^\mu(K) B_{\mu\nu}(K) \tilde{x}^\nu(K)} + \delta S(x, K), \quad (48)$$

where we adjust the parameters  $N(K)$ ,  $\bar{x}^\mu(K)$ , and  $B_{\mu\nu}(K)$  of the Gaussian first term in such a way that the correction term  $\delta S$  has vanishing zeroth, first and second order space-time moments:

$$\int d^4x \delta S(x, K) = \int d^4x x^\mu \delta S(x, K) = \int d^4x x^\mu x^\nu \delta S(x, K) = 0. \quad (49)$$

This is achieved by choosing

$$N(K) = E_K \frac{dN}{d^3K} \frac{\det B_{\mu\nu}(K)}{S(\bar{x}(K), K)}, \quad (50)$$

$$\bar{x}^\mu(K) = \langle x^\mu \rangle, \quad (51)$$

$$(B^{-1})_{\mu\nu}(K) = \langle \tilde{x}_\mu \tilde{x}_\nu \rangle \equiv \langle (x - \bar{x})_\mu (x - \bar{x})_\nu \rangle. \quad (52)$$

The ( $K$ -dependent) average over the source function  $\langle \dots \rangle$  has been defined in Eq. (42). The normalization factor (50) ensures that the Gaussian term in (48) gives the correct

single-particle spectrum (38); it fixes the normalization on-shell, i.e. for  $K^0 = E_K$ , but as we discussed this is where we need the emission function also for the computation of the correlator. (Note that for photon interferometry this may not be true, and (50) should then be replaced by a suitable generalization.)  $\bar{x}(K)$  in (51) is the centre of the emission function  $S(x, K)$  and approximately equal to its “saddle point”, i.e. the point of highest emissivity for particles with momentum  $K$ . The second equality in (52) defines  $\tilde{x}$  as the space-time coordinate relative to the centre of the emission function; only this quantity enters the further discussion, since, due to the invariance of the momentum spectra under arbitrary translations of the source in coordinate space, the absolute position of the emission point is not measurable in experiments which determine only particle momenta. Since  $\bar{x}(K)$  is not measurable, neither is the normalization  $N(K)$  [23] as its definition (50) involves the emission function at  $\bar{x}(K)$ . Finally, Eq. (52) ensures that the Gaussian first term in (48) correctly reproduces the variances  $\langle \tilde{x}_\mu \tilde{x}_\nu \rangle$  of the original emission function, in particular its r.m.s. widths in the various space-time directions.

Inserting the decomposition (48) into Eq. (42) we obtain for the correlation function

$$C(\mathbf{q}, \mathbf{K}) = 1 + \exp[-q^\mu q^\nu \langle \tilde{x}_\mu \tilde{x}_\nu \rangle(\mathbf{K})] + \delta C(\mathbf{q}, \mathbf{K}). \quad (53)$$

The Gaussian in  $q$  results from the Fourier transform of the Gaussian contribution in (48); the last term  $\delta C$  receives contributions from the second term  $\delta S$  in (48) which contains information on the third and higher order space-time moments of the emission function, like sharp edges, wiggles, secondary peaks, etc. in the source. It is at least of fourth order in  $q$ , i.e. the second derivative of the full correlator at  $q = 0$  is given *exactly* by the Gaussian in (53). Please note that the exponent of the correlator contains no term linear in  $q$ ; since the correlator must be symmetric under  $\mathbf{q} \rightarrow -\mathbf{q}$  because it does not matter which of the two particles of the pair receives the label 1 or 2, a linear  $q$ -dependence could only arise in the form  $\exp(-R|\mathbf{q}|)$ . The only type of emission function yielding such a  $q$ -dependence of the correlator would be a spherically symmetric Lorentzian. Any emission function which at large  $x$  falls off faster than  $1/x^2$  results in the leading Gaussian behaviour (53) instead. This settles, in my opinion, the old issue whether Gaussian or exponential fits of the correlation function should be preferred.

[In the past it has repeatedly been observed that the correlation data appear to be better fit by exponentials than by Gaussians. However, as far as I know, this happened always when one tried to fit the correlator as a function of the single Lorentz invariant variable  $Q_{\text{inv}}^2 = (q^0)^2 - \mathbf{q}^2$ . Contemplating the structure of Eq. (53) one realizes that such a fit does not make sense: the generic structure of the exponent,  $-q^\mu q^\nu \langle \tilde{x}_\mu \tilde{x}_\nu \rangle$ , tells us that the term  $(q^0)^2$  should come with the time variance of the source while the spatial components  $(q^i)^2$  should come with the spatial variances of the source. Since all variances are positive semidefinite by definition, it does not make sense to parametrize the correlation function by a variable in which  $(q^0)^2$  and  $\mathbf{q}^2$  appear with the opposite sign! Such a fit could only work if the time variance and all mixed variances would vanish identically, and all three spatial variances were equal. This is certainly not the general case in nature. The good exponential fits of the correlation functions from  $pp$  and  $e^+e^-$  collisions are thus, in my mind, purely accidental and an empirical curiosity without physical meaning. *The variable  $Q_{\text{inv}}$  should not be used for fitting HBT data.*]

Please note also that Eq. (53) has no factor  $\frac{1}{2}$  in the exponent. If the measured correlator is fitted by a Gaussian as defined in (53), its  $q$ -width can be directly interpreted in terms of the r.m.s. widths of the source in coordinate space. Any remaining factors of  $\sqrt{3}$ ,  $\sqrt{3}$ , or  $\sqrt{5}$  (which you can sometimes find in the literature) are due to reexpressing the r.m.s. width of the source in terms of certain other width parameters chosen for

the parametrization of the source in coordinate space. The confusion connected with such factors is easily avoided by always expressing the source parametrization directly in terms of r.m.s. widths.

Eqs. (48) and (53) would, of course, not be useful if the contributions from  $\delta S$  and  $\delta C$  were not somehow small enough to be neglected. This requires a numerical investigation. It was shown numerically in Ref. [19] that in typical (and even in some not so typical) situations  $\delta S$  has a negligible influence on the half width of the correlation function. It contributes only weak, essentially unmeasurable structures in  $C(\mathbf{q}, \mathbf{K})$  at large values of  $\mathbf{q}$ . The reader can easily verify this analytically for an emission function with a sharp box profile; the results for the exact correlator and the one resulting from the Gaussian approximation (48) are given in [18] and differ by less than 5% in the half widths; the exact correlator has, as a function of  $q$ , secondary maxima with an amplitude below 5% of the value of the correlator at  $q = 0$ . We have checked that similar statements remain even true for a source with a doughnut structure, i.e. with a hole in the middle, which was obtained by rotating the superposition of two 1-dimensional Gaussians separated by twice their r.m.s. widths around their center. The only situation where these statements require qualification is if the correlator receives contributions from the decay of long-lived resonances; this will be discussed in Lecture 3.

From Eq. (53) we conclude that the two-particle correlation function measures the second order space-time variances of the emission function. That's it – finer features of its space-time structure (edges, wiggles, holes) cannot be measured with two-particle correlations. The variances  $\langle \tilde{x}_\mu \tilde{x}_\nu \rangle$  are in general *not* identical with our naive intuitive notion of the “source radius”: unless the source is stationary and has no  $x$ - $K$ -correlations at all, the variances depend on the momentum  $\mathbf{K}$  of the pair and cannot be interpreted in terms of simple overall source geometry. Their correct physical interpretation [25, 21, 14] is in terms of “lengths of homogeneity” which give, for each pair momentum  $\mathbf{K}$ , the size of the region around the point of maximal emissivity  $\bar{x}(\mathbf{K})$  over which the emission function is sufficiently homogeneous to contribute to the correlation function. Thus HBT measures “regions of homogeneity” in the source and their variation with the momentum of the particle pairs. As we will see, the latter is the key to their physical interpretation.

### 3.4. Gaussian parametrizations for the correlation function

A full characterization of the source in terms of its second order space-time variances requires knowledge of the 10 parameters  $\langle \tilde{x}_\mu \tilde{x}_\nu \rangle$ . These quantities appear in the expression (42) for the correlation function but this expression still uses all four components of the relative momentum  $q^\mu$ . However, as already noted only three of the four components are independent, due to the mass-shell constraint (45). Thus only 6 linear combinations of the variances  $\langle \tilde{x}_\mu \tilde{x}_\nu \rangle(\mathbf{K})$  are actually measurable [18].

If the source is azimuthally symmetric around the beam axis, this counting changes as follows: Even if the source is azimuthally symmetric in coordinate space, the emission function  $S(x, K)$  in phase space is for finite  $\mathbf{K}$  no longer azimuthally symmetric because the transverse components  $\mathbf{K}_\perp$  of the pair momentum distinguish a direction transverse to the beam direction. There remains, however, a reflection symmetry with respect to the plane spanned by  $\mathbf{K}$  and the beam axis. If we call the direction orthogonal to this plane  $y$ , all mixed variances which are linear in  $y$  must vanish due to this reflection symmetry, and the correlator must be symmetric under  $q_y \rightarrow -q_y$ . Thus only 7 non-vanishing variances  $\langle \tilde{x}_\mu \tilde{x}_\nu \rangle$  survive in general, of which, due to the mass-shell constraint

(45) only 4 linear combinations are measurable.

Before the correlator (53) can be fit to experimental data, the redundant components of  $q$  must first be eliminated from the exponent of the Gaussian. At this point it is useful to introduce a cartesian coordinate system with  $z$  along the beam axis and  $\mathbf{K}$  lying in the  $x$ - $z$ -plane. Customarily one labels the  $z$ -component of a 3-vector by  $l$  (for *longitudinal*), the  $x$ -component by  $o$  (for *outward*) and the  $y$ -component by  $s$  (for *sideward*). The above choice of the orientation of the  $x$  and  $y$  axes is natural for azimuthally symmetric collision events or event samples because then the transverse components  $\mathbf{K}_\perp$  of the pair momentum distinguish a direction in the transverse plane, and it is convenient to orient one of the coordinate axes along this direction such that  $\mathbf{K}$  has only one transverse component:

$$\mathbf{K} = (K_x, K_y, K_z) = (K_\perp, 0, K_L). \quad (54)$$

For sources without azimuthal symmetry, e.g. from collisions at finite impact parameter which have been selected according to the orientation of the collision plane, it is probably more useful to orient the  $x$  axis along the collision plane; then  $\mathbf{K}$  will be characterized by three parameters,  $K_L$ ,  $K_\perp$  and the azimuthal angle  $\Phi$  of  $\mathbf{K}_\perp$  relative to the  $x$ - $z$  collision plane.

A useful formalism for HBT interferometry of finite impact parameter collisions has not yet been developed. I will therefore limit my discussion to azimuthally symmetric event samples and exploit the symmetry to orient the  $x$ -axis along  $\mathbf{K}_\perp$ . Then from (45) we see that  $\beta_s = 0$  such that

$$q^0 = \beta_\perp q_o + \beta_l q_l \quad (55)$$

with  $\beta_\perp = |\mathbf{K}_\perp|/K^0$  being (approximately) the velocity of the particle pair transverse to the beam direction while  $\beta_l$  is its longitudinal component.

This constraint can now be used in various ways to eliminate the redundant  $q$ -components from the exponent of Eq. (53). But whichever choice one makes, all the  $\mathbf{K}$ -dependent parameters (“HBT radii”) in the resulting Gaussian function of  $q$  can be easily calculated from the variances  $\langle \tilde{x}^\mu \tilde{x}^\nu \rangle$ , i.e. by simple quadrature formulae, for arbitrary emission functions  $S(x, K)$ . The relation between the HBT parameters and the variances is *model-independent*, i.e. it does not depend on the form of the emission function  $S(x, K)$ .

Here I discuss two specific parametrizations: the standard Cartesian one (mostly for historic reasons [13, 26, 27, 20]), and the more physically motivated Yano-Koonin-Podgoretskiĭ one [18, 23, 24].

#### 3.4.1. Standard Cartesian parametrization

The standard form [14, 20] for the parametrization of the correlation function is obtained by using (55) to eliminate  $q^0$  from Eq. (53). One obtains

$$C(\mathbf{q}, \mathbf{K}) = 1 + \exp \left[ - \sum_{i,j=s,o,l} R_{ij}^2(\mathbf{K}) q_i q_j \right] \quad (56)$$

where the 6 HBT radius parameters  $R_{ij}$  are defined in terms of the following variances of the source function [14, 20, 28]:

$$R_{ij}^2(\mathbf{K}) = \langle (\tilde{x}_i - \beta_i \tilde{t})(\tilde{x}_j - \beta_j \tilde{t}) \rangle, \quad i, j = s, o, l. \quad (57)$$

For an azimuthally symmetric sample of collision events  $C(\mathbf{q}, \mathbf{K})$  is symmetric with respect to  $q_s \rightarrow -q_s$  [ 18]. Then  $R_{os}^2 = R_{sl}^2 = 0$  and

$$C(\mathbf{q}, \mathbf{K}) = 1 + \exp \left[ -R_s^2(\mathbf{K})q_s^2 - R_o^2(\mathbf{K})q_o^2 - R_l^2(\mathbf{K})q_l^2 - 2R_{ol}^2(\mathbf{K})q_oq_l \right], \quad (58)$$

with

$$R_s^2(\mathbf{K}) = \langle \tilde{y}^2 \rangle, \quad (59)$$

$$R_o^2(\mathbf{K}) = \langle (\tilde{x} - \beta_\perp \tilde{t})^2 \rangle, \quad (60)$$

$$R_l^2(\mathbf{K}) = \langle (\tilde{z} - \beta_l \tilde{t})^2 \rangle, \quad (61)$$

$$R_{ol}^2(\mathbf{K}) = \langle (\tilde{x} - \beta_\perp \tilde{t})(\tilde{z} - \beta_l \tilde{t}) \rangle. \quad (62)$$

The cross-term (62) was only recently discovered [ 20]. Clearly these HBT radius parameters mix spatial and temporal information on the source in a non-trivial way. Furthermore, since they multiply combinations of the components  $q^\mu$  which are not invariant under longitudinal boosts of the measurement frame, their interpretation depends on the frame in which the particle momenta are specified. This complicates their physical interpretation. An extensive discussion of these parameters, in particular of the meaning of the generally non-vanishing cross-term  $R_{ol}^2$ , can be found in Refs. [ 14, 18, 19, 20, 29, 30], where the expressions (59)-(62) were analyzed analytically and numerically for a large class of (azimuthally symmetric) model source functions. Some of these results will be discussed in the Lecture 3.

An important observation resulting from these studies is that the difference

$$R_{\text{diff}}^2 \equiv R_o^2 - R_s^2 = \beta_\perp^2 \langle \tilde{t}^2 \rangle - 2\beta_\perp \langle \tilde{x}\tilde{t} \rangle + (\langle \tilde{x}^2 \rangle - \langle \tilde{y}^2 \rangle) \quad (63)$$

is generally dominated by the first term on the r.h.s. and thus provides access to the lifetime  $\Delta t = \sqrt{\langle \tilde{t}^2 \rangle - \langle \tilde{t} \rangle^2}$  of the source (more exactly: the duration of the particle emission process) [ 31]. However, in relativistic heavy-ion collisions, due to rapid expansion of the source one would not expect  $\langle \tilde{t}^2 \rangle$  to be generically much larger than either  $\langle \tilde{x}^2 \rangle$  or  $\langle \tilde{y}^2 \rangle$  unless there is a phase transition to a quark-gluon plasma and the collision fireball is initiated within a certain range of energy densities above the critical energy density where the transition occurs [ 32]. In the standard fit one is not sensitive to small values of  $\Delta t$  since Eq. (63) then involves a small difference of two large numbers, each associated with standard experimental errors. The factor  $\beta_\perp^2 \leq 1$  in front of  $\langle \tilde{t}^2 \rangle$  further complicates its extraction, in particular at low  $K_\perp$  where  $\Delta t(\mathbf{K})$  is usually largest (see below). Successful attempts to determine the duration of particle emission from HBT measurements have been reported from low-energy heavy-ion collisions (using 2-proton correlations) where the measured lifetimes are very long:  $25 \pm 15$  fm/c in Ar+Sc collisions at  $E/A = 80$  MeV [ 33] and  $1400 \pm 300$  fm/c in Xe+Al collisions at  $E/A = 31$  MeV [ 34] (the latter is the typical evaporation time of a compound nucleus). Two-pion correlations at ultra-relativistic energies ( $E/A = 200$  GeV) so far failed to yield positive evidence for a non-vanishing emission duration [ 35, 36], except for the heaviest collision system Pb+Pb [ 37], but even there the effective lifetime is only a few fm/c.

### 3.4.2. Yano-Koonin-Podgoretskiĭ (YKP) parametrization

The Yano-Koonin-Podgoretskiĭ parametrization of the correlation function is the generalization to azimuthally symmetric systems of the Yano-Koonin parametrization [ 38]. It was first written down by M.I. Podgoretskiĭ in 1983 for moving azimuthally

symmetric, but non-expanding sources [ 39], with  $K$ -independent parameters. Not knowing about this paper, we reinvented it in [ 18], with  $K$ -dependent parameters for expanding azimuthally symmetric systems. The YKP parametrization is based on an elimination in Eq. (53) of  $q_o$  and  $q_s$  in terms of  $q_\perp = \sqrt{q_o^2 + q_s^2}$ ,  $q^0$ , and  $q_3$ , using Eq. (55):

$$C(\mathbf{q}, \mathbf{K}) = 1 + \exp \left[ -R_\perp^2 q_\perp^2 - R_\parallel^2 (q_\parallel^2 - (q^0)^2) - (R_0^2 + R_\parallel^2) (q \cdot U)^2 \right]. \quad (64)$$

Like the standard Cartesian form (58) it has four  $K$ -dependent fit parameters, but now only three of them,  $R_\perp(\mathbf{K})$ ,  $R_\parallel(\mathbf{K})$ , and  $R_0(\mathbf{K})$ , have dimensions of length while the fourth parameter,  $U(\mathbf{K})$ , is a 4-velocity with only a longitudinal spatial component:

$$U(\mathbf{K}) = \gamma(\mathbf{K}) (1, 0, 0, v(\mathbf{K})), \quad \text{with } \gamma = \frac{1}{\sqrt{1 - v^2}}. \quad (65)$$

This parametrization has the advantage that the ‘‘YKP radii’’  $R_\perp$ ,  $R_\parallel$ , and  $R_0$  extracted from such a fit do not depend on the longitudinal velocity of the observer system in which the correlation function is measured; they are invariant under longitudinal boosts. Their physical interpretation is easiest in terms of coordinates measured in the frame where  $v(\mathbf{K})$  vanishes. There they are given by [ 18]

$$R_\perp^2(\mathbf{K}) = R_s^2(\mathbf{K}) = \langle \tilde{y}^2 \rangle, \quad (66)$$

$$R_\parallel^2(\mathbf{K}) = \langle (\tilde{z} - \beta_t \tilde{x} / \beta_\perp)^2 \rangle - \beta_t^2 \langle \tilde{y}^2 \rangle / \beta_\perp^2 \approx \langle \tilde{z}^2 \rangle, \quad (67)$$

$$R_0^2(\mathbf{K}) = \langle (\tilde{t} - \tilde{x} / \beta_\perp)^2 \rangle - \langle \tilde{y}^2 \rangle / \beta_\perp^2 \approx \langle \tilde{t}^2 \rangle, \quad (68)$$

where in the last two expressions the approximation consists of dropping terms which were found in [ 18] to be generically small. (A more quantitative discussion of this point will follow in Lecture 3.) The first expression (66) remains true in any longitudinally boosted frame.

Eq. (68) shows that the YKP parameter  $R_0(\mathbf{K})$  essentially measures the time duration  $\Delta t(\mathbf{K}) = \sqrt{\langle \tilde{t}^2 \rangle}$  during which particles of momentum  $\mathbf{K}$  are emitted, in the frame where the YKP velocity  $v(\mathbf{K}) = 0$ . It enters as the leading contribution in  $R_0$ , is fitted directly and no longer obtained as the difference of two large fit parameters as in the standard Cartesian fit.

Eqs. (66)-(68) were written down in the special frame where  $v(\mathbf{K}) = 0$  which we call the *Yano-Koonin (YK) frame*. In Refs. [ 18, 24] it is shown that for a large class of models this frame essentially coincides with the longitudinal rest frame of the fluid cell around the point  $\bar{x}(\mathbf{K})$  of maximum emissivity at momentum  $\mathbf{K}$  (i.e. the *Longitudinal Saddle Point System* LSPS [ 22]). This is true also for sources which are not longitudinally boost-invariant and for which the LSPS and the LCMS (the *Longitudinally CoMoving System* in which the pion pair has  $\beta_t = 0$  [ 31]) do not coincide.

In general the measurement system will not coincide with the ( $K$ -dependent) YK-frame, and the YKP radii will be given by more complicated combinations of the space-time variances of the source expressed in the coordinates of the measurement frame. This is the simple result of a Lorentz-boost between the two frames. However, I stress that in any frame the YKP parameters can again be easily calculated from the second order moments of the source function  $S(x, K)$ , i.e. by simple quadrature. Introducing the notational shorthands

$$A = \left\langle (\tilde{t} - \tilde{\xi} / \beta_\perp)^2 \right\rangle, \quad (69)$$

$$B = \left\langle \left( \tilde{z} - \beta_l \tilde{\xi} / \beta_\perp \right)^2 \right\rangle, \quad (70)$$

$$C = \left\langle \left( \tilde{t} - \tilde{\xi} / \beta_\perp \right) \left( \tilde{z} - \beta_l \tilde{\xi} / \beta_\perp \right) \right\rangle, \quad (71)$$

where  $\tilde{\xi} \equiv \tilde{x} + i\tilde{y}$  and  $\langle \tilde{y} \rangle = \langle \tilde{x}\tilde{y} \rangle = 0$  for azimuthally symmetric sources such that  $\langle \tilde{\xi}^2 \rangle = \langle \tilde{x}^2 - \tilde{y}^2 \rangle$ , one finds in an arbitrary longitudinal reference frame

$$v = \frac{A+B}{2C} \left( 1 - \sqrt{1 - \left( \frac{2C}{A+B} \right)^2} \right), \quad (72)$$

$$R_{\parallel}^2 = \frac{1}{2} \left( \sqrt{(A+B)^2 - 4C^2} - A + B \right) = B - vC, \quad (73)$$

$$R_0^2 = \frac{1}{2} \left( \sqrt{(A+B)^2 - 4C^2} + A - B \right) = A - vC. \quad (74)$$

The Yano-Koonin velocity  $v$  is zero in the frame where the expression (71) for  $C$  vanishes [ 18]; this fixes also the sign in front of the square root in (72). For small values of  $C$  the Yano-Koonin velocity is given approximately by

$$v \approx \frac{C}{A+B} \approx \frac{\langle \tilde{z}\tilde{t} \rangle}{\langle \tilde{t}^2 \rangle + \langle \tilde{z}^2 \rangle}, \quad (75)$$

where in the second approximation we again neglected generically small terms [ 18] proportional to  $\langle \tilde{z}\tilde{x} \rangle$ ,  $\langle \tilde{x}\tilde{t} \rangle$ , and  $\langle \tilde{x}^2 - \tilde{y}^2 \rangle$ . The accuracy of the approximate expression (75) for  $v(\mathbf{K})$  was tested numerically in [ 24] and found to be excellent in the situations discussed below. In the same limit the expressions for  $R_0^2$  and  $R_{\parallel}^2$  simplify to  $R_0^2 \approx A$  and  $R_{\parallel}^2 \approx B$ , in agreement with (67) and (68).

Since the standard Cartesian and YKP parametrizations are mathematically equivalent (being simply based on a different choice of independent  $q$ -components), the resulting HBT parameters obey simple relations [ 23]:

$$R_s^2 = R_\perp^2, \quad (76)$$

$$R_{\text{diff}}^2 = R_o^2 - R_s^2 = \beta_\perp^2 \gamma^2 \left( R_0^2 + v^2 R_{\parallel}^2 \right), \quad (77)$$

$$R_l^2 = \left( 1 - \beta_l^2 \right) R_{\parallel}^2 + \gamma^2 \left( \beta_l - v \right)^2 \left( R_0^2 + R_{\parallel}^2 \right), \quad (78)$$

$$R_{ol}^2 = \beta_\perp \left( -\beta_l R_{\parallel}^2 + \gamma^2 \left( \beta_l - v \right)^2 \left( R_0^2 + R_{\parallel}^2 \right) \right). \quad (79)$$

Although a mathematical triviality, these relations provide a powerful consistency check on the experimental fitting procedure, of similar value as the relation [ 18, 19]  $\lim_{K_\perp \rightarrow 0} (R_o(\mathbf{K}) - R_s(\mathbf{K})) = 0$  which results from azimuthal symmetry.

#### 4. LECTURE 3: HBT CORRELATIONS FOR EXPANDING SOURCES

In this third lecture I will present a quantitative discussion of the HBT parameters, both in the standard Cartesian and in the YKP fits. The emphasis will be on their  $K$ -dependence because, as discussed in the previous two lectures, only a careful study of this pair-momentum dependence permits a separation of the geometric from the dynamic aspects of the source. You probably remember that at the beginning of Lecture 2 I stressed that a model-independent reconstruction of the emission function from HBT measurements is not possible. Therefore any quantitative discussion must necessarily occur within the framework of specific source models.

I will choose a relatively simple analytical parametrization of the emission function which was first suggested by T. Csörgő and B. Lörstad in 1994 in an unpublished preprint (see also [ 22, 20, 14, 18]) and which incorporates many of the (as we believe) relevant physical features of the typical sources created in relativistic nuclear collisions: approximate thermalization at decoupling, finite transverse and longitudinal extension of the source, collective expansion in both the longitudinal and transverse directions, and a finite duration of the particle emission process. All these features are controlled by parameters which can be freely tuned, thus allowing for extensive parameter studies [ 18, 19, 24, 30] which have given us a good intuitive understanding of which properties of the source are important for the correlation function and which aren't, and how to look in the correlation function for specific space-time properties of the emitter.

#### 4.1. A simple model for an expanding source

Let us consider the following model for the emission function [ 18, 22]:

$$S(x, K) = \frac{2J + 1}{(2\pi)^3} K \cdot n(x) \exp \left[ -\frac{K \cdot u(x) - \mu(x)}{T(x)} \right] H(x) \quad (80)$$

with

$$H(x) = \frac{1}{\pi \Delta \tau} \exp \left[ -\frac{r^2}{2R^2} - \frac{(\eta - \eta_0)^2}{2(\Delta \eta)^2} - \frac{(\tau - \tau_0)^2}{2(\Delta \tau)^2} \right] \quad (81)$$

and

$$K \cdot n(x) = M_{\perp} \cosh(\eta - Y). \quad (82)$$

The factor  $2J + 1$  counts the spin degeneracy of the observed particle species and is included because the detectors usually do not identify the polarization of the measured particles. There is no such factor for isospin because of the requirement that the two particles in the pair be identical, i.e. have the, for example, the same electric charge. The Lorentz covariant Boltzmann factor  $\exp[-(K \cdot u(x) - \mu(x))/T(x)]$  implements the assumption of local thermal equilibrium of the emitted particles at freeze-out, with local temperature  $T(x)$  and chemical potential  $\mu(x)$ , and the collective expansion of the source with hydrodynamic flow 4-velocity  $u_{\mu}(x)$ . I will here take  $T$  and  $\mu$  as constants and refer to Refs. [ 22, 30] for an investigation of the effects of temperature gradients. The factor  $H(x)$  describes the geometric properties of the source; it can be interpreted as a space-time modulation of the fugacity  $\exp[\mu(x)/T(x)]$ . Space-time is parametrized by *longitudinal proper time*  $\tau = \sqrt{t^2 - z^2}$  and *space-time rapidity*  $\eta = \frac{1}{2} \ln[(t + z)/(t - z)]$  in the longitudinal and temporal directions, and by  $r = \sqrt{x^2 + y^2}$  and  $\phi$  in the transverse directions. The volume element is then  $d^4x = \tau d\tau d\eta r dr d\phi$ . The Gaussian factors  $\exp[-r^2/(2R^2)]$  and  $\exp[-(\eta - \eta_0)^2/(2(\Delta \eta)^2)]$  provide smooth geometric limits for the source in the transverse and longitudinal directions, scaled by  $R$  and  $L = \tau \Delta \eta$ , respectively. The function  $H(x)$  is normalized to the total comoving 3-volume according to

$$\int d^4x H(x) = \pi r_{\text{rms}}^2 \cdot 2\tau_0 \eta_{\text{rms}} \quad (83)$$

where

$$r_{\text{rms}}^2 = 2R^2 = x_{\text{rms}}^2 + y_{\text{rms}}^2, \quad \eta_{\text{rms}} = \Delta \eta \quad (84)$$

are the r.m.s. expectation values for the transverse radius  $r$  and for  $\eta$ , respectively. (The r.m.s. widths for  $x$  and  $y$  are each given by  $R$ .) If the Gaussians in  $H(x)$  were replaced by box functions, the equivalent box dimensions (with the same r.m.s. radii) would be  $\tilde{R} = 2R$ ,  $\tilde{\eta} = \sqrt{3}\Delta \eta$ . (Here you see the “unnecessary” factors  $\sqrt{2}$  and  $\sqrt{3}$  mentioned before!)

$K \cdot n(x)$  is the flux factor through the freeze-out hypersurfaces whose normal direction is given by the unit vector  $n_\mu(x)$ . In our model these hypersurfaces are for simplicity assumed to be surfaces of constant longitudinal proper time  $\tau$ , parametrized by surface coordinates  $\Sigma_{(\tau)}(x) = (\tau \cosh \eta, r \cos \phi, r \sin \phi, \tau \sinh \eta)$ . The last factor in  $H(x)$  provides a Gaussian smearing of the proper time around the mean values  $\tau_0$  with dispersion  $\Delta\tau$ , thereby implementing particle emission over a finite time interval of order  $\Delta\tau$  in the local comoving frame. With these assumptions the flux factor reduces [18] to the form given in Eq. (82). For  $\Delta\tau \rightarrow 0$  the Gaussian in  $\tau$  approaches a  $\delta$ -function centered at  $\tau_0$ , simulating instantaneous freeze-out at constant proper time as often implemented in hydrodynamical situations.

[Let me make some side remarks on hydrodynamical simulations here, because they are a very popular tool for computing the space-time dynamics of the reaction zone in heavy-ion collisions. In hydrodynamics freeze-out is always assumed to occur on a sharp hypersurface (not a smeared one as here), and one writes the emission function in the form [40]

$$S(x, K) = \frac{2J+1}{(2\pi)^3} \int_{\Sigma} \frac{K^\mu d^3\sigma_\mu(x') \delta^{(4)}(x-x')}{\exp[(K \cdot u(x') - \mu(x'))/T(x')] \pm 1}, \quad (85)$$

where  $d^3\sigma_\mu(x')$  is the normal vector on the freeze-out surface  $\Sigma(x')$ , and we have correctly accounted for the quantum statistical effects in the local thermal distribution functions. The latter are unimportant for heavy particles but should, in a quantitative comparison with data, be included for pions – at least in the single-particle spectrum. Inserting the ansatz (85) into the expression (38) for the single-particle spectrum one obtains the well-known Cooper-Frye formula [41]

$$E_K \frac{dN}{d^3K} = \int_{\Sigma} K^\mu d^3\sigma_\mu(x) f(x, p) \quad (86)$$

with the local equilibrium distribution function

$$f(x, p) = \frac{2J+1}{(2\pi)^3} \frac{1}{\exp[(K \cdot u(x) - \mu(x))/T(x)] \pm 1}. \quad (87)$$

For the numerator of the correlator in (39) one obtains

$$\int_{\Sigma} K^\mu d^3\sigma_\mu(x) K^\nu d^3\sigma_\nu(y) f(x, K) f(y, K) \exp[iq \cdot (x - y)], \quad (88)$$

similar, but not identical with to the one given in [42]. In [42] each of the two distribution functions under the integral featured on-shell arguments  $p_a$  and  $p_b$ , respectively, instead of the common (off-shell) average argument  $K$  as in (88). This error in [42] can be traced back to an inaccurate transition from finite discrete volumes along the freeze-out surface  $\Sigma$  to the continuum limit [43]. Taking over this inaccuracy produces (in particular for very rapidly expanding sources) unphysical oscillations of the correlation function around unity at large values of  $\mathbf{q}$  (see e.g. [8]) which are inconsistent with the manifestly positive definite nature of the exchange term noted in Lecture 1. Recently Aichelin [44] pointed out that, for technical reasons, the same erroneous assumption is made in all simulations of HBT correlations using Monte Carlo event generators. This problem should certainly receive more attention in the future.]

Since according to Eq. (41) the time-component of the pair momentum may be approximated by the on-shell value  $K_0 = E_K = \sqrt{m^2 + \mathbf{K}^2}$ , the pair momentum  $K$  can

be parametrised in terms of the momentum rapidity  $Y = \frac{1}{2} \ln[(1 + \beta_l)/(1 - \beta_l)]$  and the transverse mass  $M_\perp = \sqrt{m^2 + K_\perp^2}$ ,

$$K^\mu = (M_\perp \cosh Y, K_\perp, 0, M_\perp \sinh Y). \quad (89)$$

We implement longitudinal and azimuthally symmetric transverse expansion of the source by parametrising the flow velocity in the form

$$u^\mu(x) = \left( \cosh \eta_l(\tau, \eta) \cosh \eta_t(r), \frac{x}{r} \sinh \eta_t(r), \frac{y}{r} \sinh \eta_t(r), \sinh \eta_l(\tau, \eta) \cosh \eta_t(r) \right). \quad (90)$$

For the longitudinal flow rapidity we take  $\eta_l(\tau, \eta) = \eta$  independent of  $\tau$ , i.e. we assume a Bjorken scaling profile [45]  $v_l = z/t$  in the longitudinal direction. The growth of the longitudinal flow velocity in the longitudinal direction is then automatically limited by the Gaussian in  $\eta$  in (81). For the transverse flow rapidity we take a linear profile of strength  $\eta_f$ :

$$\eta_t(r) = \eta_f \left( \frac{r}{R} \right). \quad (91)$$

The scalar product in the exponent of the Boltzmann factor can then be written as

$$K \cdot u(x) = M_\perp \cosh(\eta - Y) \cosh \eta_t(r) - K_\perp \frac{x}{r} \sinh \eta_t(r), \quad (92)$$

Please note that for non-zero transverse momentum  $K_\perp$ , a finite transverse flow breaks the azimuthal symmetry of the emission function via the second term in (92). For  $\eta_f = 0$  the source has no explicit  $K_\perp$ -dependence, and  $M_\perp$  is the only relevant scale. As will be discussed later this gives rise to perfect  $M_\perp$ -scaling of the YKP radius parameters in the absence of transverse flow, which is again broken for non-zero transverse flow [46].

Besides  $\eta_f$ , the model parameters are the freeze-out temperature  $T$ , the transverse geometric (Gaussian) radius  $R$ , the average freeze-out proper time  $\tau_0$  as well as the mean proper emission duration  $\Delta\tau$ , the centre of the source rapidity distribution  $\eta_0$ , and the (Gaussian) width of the space-time rapidity profile  $\Delta\eta$ . A rough spatial picture of the source at various fixed coordinate times can be gleaned from Figs. 1 and 2 in Ref. [47] to which I would like to refer those readers having trouble with visualizing Gaussians in  $\eta$  and  $\tau$  in regular Cartesian coordinates. Although the source in Ref. [47] has sharp edges in space and time whereas ours is smoothed by Gaussian profiles, the essential space-time features of the sources are very similar.

The calculations presented below were done for pions ( $m = m_{\pi^\pm} = 139 \text{ MeV}/c^2$ ) and kaons ( $m = m_{K^\pm} = 494 \text{ MeV}/c^2$ ) and (except where noted otherwise) for the fixed set of parameters  $T = 140 \text{ MeV}$ ,  $R = 3 \text{ fm}$ ,  $\tau_0 = 3 \text{ fm}/c$ ,  $\Delta\tau = 1 \text{ fm}/c$ ,  $\Delta\eta = 1.2$ , and  $\eta_0 = 0$  (i.e. all our rapidities will be given relative to the rapidity  $\eta_0$  of the c.m. of the source). The strength  $\eta_f$  of the transverse flow will be varied systematically to investigate its effects on the HBT parameters. A detailed discussion of how the variation of some of the other parameters affects the correlation function can be found in Refs. [24, 30].

## 4.2. $K$ -dependence of the HBT radii

### 4.2.1. Analytical approximations – HBT radii as lengths of homogeneity

For a qualitative understanding of the physical origin of the pair-momentum dependence of the HBT parameters it is instructive to start from their model-independent

expressions in terms of space-time variances and evaluate the latter approximately analytically. For the standard Cartesian fit parameters (59)-(62) this was done, at different levels of accuracy, in Refs. [ 14, 19, 21, 22] by exploiting the method of saddle-point integration for the evaluation of the variances. This method was introduced by Makhlin and Sinyukov [ 25] in the context of infinitely long sources with boost-invariant longitudinal expansion where they used it to show that the longitudinal HBT radius  $R_l$  is

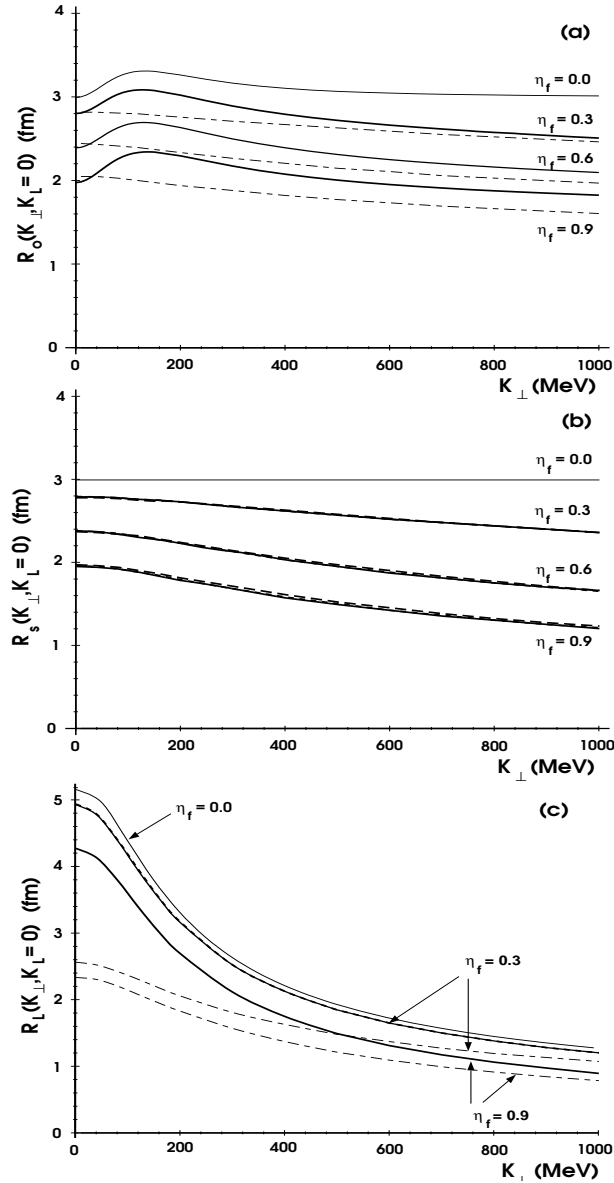


**Fig.1.**  $K_{\perp}$ -dependence of the standard Cartesian HBT radii  $R_o$  (top),  $R_s$  (middle), and  $R_l$ , evaluated in the LCMS (the frame where  $K_L = 0$ ), for an infinitely long source ( $\Delta\eta \rightarrow \infty$  in Eqs. (80,81)) with boost-invariant longitudinal expansion and a linear transverse flow rapidity profile. The strength of the transverse flow  $\eta_f$  is varied between  $\eta_f = 0$  and  $\eta_f = 0.9$  as indicated. The duration parameter  $\Delta\tau$  was set to 0 (locally instantaneous freeze-out). For such a source the cross-term  $R_{ol}$  vanishes identically in the LCMS. Solid lines represent results from a full numerical evaluation of the integrals in Eqs. (59-62). Dashed lines give the results from the leading-order saddle-point approximation to these integrals. One sees that the saddle-point integration misses the rise of  $R_o$  at small  $K_{\perp}$  (i.e. the contribution from the finite duration of particle emission in the LCMS frame, see text) and gives a very bad approximation to  $R_l$  at small  $K_{\perp}$ . The solid line for  $R_l$  for  $\eta_f = 0$  is given analytically by  $R_l = \tau_0 \sqrt{T/M_{\perp}} \sqrt{K_2(M_{\perp}/T)/K_1(M_{\perp}/T)}$  [ 28] while the saddle-point approximation (dashed) gives for  $\eta_f = 0$  the Makhlin-Sinyukov formula  $R_l = \tau_0 \sqrt{T/M_{\perp}}$  [ 25]. (Figure taken from Ref. [ 19].)

finite and determined by the inverse of the longitudinal velocity gradient, noting for the first time that  $R_l$  has the property of a “longitudinal length of homogeneity” in the source rather than being related to the longitudinal geometric size of the entire source. It was later observed [ 14, 19] that not all of the important qualitative features of the  $K$ -dependence of the HBT parameters can be obtained from the leading term in the saddle point approximation (see Fig. 1). In particular, in the presence of transverse flow the saddle point moves away from the beam axis  $r = 0$ , and this must be taken into account in order to obtain reasonable approximations [ 19]. Unfortunately, this renders the whole procedure rather cumbersome [ 19], and in the end, e.g. for a quantitative comparison with data, a full numerical evaluation of the integrals for the variances cannot be avoided.

In spite of their unreliability on a quantitative level, the analytical results from saddle-point integration are still very instructive on a qualitative level. I will here discuss the leading results for a longitudinally finite ( $L = \tau_0 \Delta\eta$ ) source of type (80) in the limit  $\Delta\tau = 0$ , in the LCMS (i.e. in the Longitudinally CoMoving System where the pairs have  $K_L = 0$ ). One finds [ 14]

$$R_s^2(M_{\perp}, K_L = 0) = R_*^2, \quad (93)$$

$$R_o^2(M_{\perp}, K_L = 0) = R_*^2 + \beta_{\perp}^2 (\Delta t_*)^2, \quad (94)$$

$$R_l^2(M_{\perp}, K_L = 0) = L_*^2, \quad (95)$$

$$R_{ol}^2(M_{\perp}, K_L = 0) = \frac{\beta_{\perp} Y}{\sqrt{2}} L_* \Delta t_* \left( \frac{L_*^2}{L^2} \right), \quad (96)$$

where  $R_*$ ,  $L_*$ , and  $\Delta t_*$  are functions of  $M_{\perp}$  defined by

$$\frac{1}{R_*^2} = \frac{1}{R^2} + \frac{1}{R_H^2}, \quad (97)$$

$$\frac{1}{L_*^2} = \frac{1}{L^2} + \frac{1}{L_H^2}, \quad (98)$$

$$\Delta t_* = \sqrt{2} \left( \sqrt{\tau_0^2 + L_*^2} - \tau_0 \right), \quad (99)$$

with the transverse and longitudinal “dynamical lengths of homogeneity”

$$R_H(M_{\perp}) = \frac{R}{\eta_f} \sqrt{\frac{T}{M_{\perp}}} = \frac{1}{\partial \eta_t(r)/\partial r} \sqrt{\frac{T}{M_{\perp}}}, \quad (100)$$

$$L_H(M_\perp) = \tau_0 \sqrt{\frac{T}{M_\perp}} = \frac{1}{\partial \cdot u_l} \sqrt{\frac{T}{M_\perp}}. \quad (101)$$

Strictly speaking, expression (100) is only valid for weak transverse flow  $\eta f \ll 1$ . In (101) we have defined the longitudinal flow 4-velocity  $u_l = (\cosh \eta_l, 0, 0, \sinh \eta_l) = (\cosh \eta, 0, 0, \sinh \eta)$ .

The physical interpretation of these results is quite interesting: in addition to geometry (implemented by the Gaussian cutoff factors in the function  $H(x)$ ), dynamics affects the HBT radii through the dynamical homogeneity lengths  $R_H, L_H$ . The latter are inversely proportional to the gradients of the expansion velocity field in the respective direction, but smeared by a thermal smearing factor  $\sqrt{T/M_\perp}$  resulting from the random thermal motion of the particles around the fluid velocity. The HBT radii are determined by the shorter of the two (geometric or dynamic) lengths scales. In the absence of random thermal motion ( $T \rightarrow 0$ ) any velocity gradient in the system would lead to a vanishing dynamical length of homogeneity and consequently to vanishing HBT radii. At finite  $T$ , the dynamical smearing decreases with increasing transverse mass  $M_\perp$ , leading to a decrease of the HBT radii at large  $M_\perp$ . (It turns out that the  $\sqrt{1/M_\perp}$ -scaling of the HBT radii at large  $M_\perp$  suggested by these analytical expressions is unreliable and a consequence of the saddle-point approximation [ 19]. A numerical analysis [ 46, 24] shows that the power of  $M_\perp$  itself, by which the HBT radii decrease for increasing  $M_\perp$ , is proportional to the expansion velocity gradient.)

The following intuitive picture results from these considerations: if the expansion velocity is small, i.e. all velocity gradients can be essentially neglected over the range where the geometric Gaussians in  $H(x)$  are large, then HBT measures the geometric parameters  $R, L$  which tell you where the function  $H(x)$  (and thus the whole emission function  $S(x, K)$ ) gets cut off. If, on the other hand, the velocity gradients are large, they effectively cut off the emission function at a distance  $R_H$  resp.  $L_H$  from the saddle point, and the matter outside these homogeneity regions decouples from the correlator because it cannot contribute particles with sufficiently small relative momenta to see the effects of quantum statistics. This explains my statement above that HBT does in general not measure the geometry of the source, but rather the regions of homogeneity inside the source at a given wavelength  $1/K$ .

Of course, a space-time dependence of the temperature field  $T(x)$  can induce additional gradients into the emission function and thus affect the size of the regions of homogeneity in the source and the HBT radii. This was investigated in some detail in Refs. [ 22, 30] to which I refer the interested reader.

The last point to be discussed is the origin of the quantity  $\Delta t_*$  in Eq. (94) for  $R_o^2$ . Comparing with Eq. (63) we see that it has the meaning of an effective source lifetime. But where does it come from, since we set the width  $\Delta\tau$  of the proper time distribution to zero? This apparent paradox has an interesting answer which is reflected in the mathematical structure of Eq. (99): since the correlator receives non-vanishing contributions from a longitudinal region of homogeneity of size  $R_l = L_*$ , it probes emission from different points  $z$  at different times  $t = \sqrt{\tau_0^2 + z^2}$  along the proper-time hyperbola  $\tau = \tau_0$ , with maximal range  $-L_* \lesssim z \lesssim L_*$ . Thus even for sharp freeze-out at constant proper time the correlator sees a non-vanishing effective lifetime in the fixed observer frame (here the LCMS) which is in principle measurable via the difference  $R_o^2 - R_s^2$ . Since  $L_*$  is a decreasing function of  $M_\perp$ , so is  $\Delta t_*$ , and for large  $M_\perp$  the difference  $R_o^2 - R_s^2$  vanishes. (If  $\Delta\tau$  were nonzero, the difference would at large  $M_\perp$  approach the limit  $(\Delta\tau)^2$ .)

#### 4.2.2. Cartesian HBT radii in the CMS and LCMS

In Fig. 2 I show the HBT radius parameters from the standard Cartesian fit (58) for pion pairs with c.m. rapidity  $Y = 1.5$  where the fit of the correlator is done in the CMS [ 30]. The different thick curves correspond to different strengths  $\eta_f$  of the transverse flow. Without transverse flow  $R_s$  is  $M_\perp$ -independent because we consider (80) for constant temperature and neglect possible transverse temperature gradients. As the transverse flow increases,  $R_s$  develops an increasing dependence on  $M_\perp$ . As shown in Fig. 6 below it can be approximated by an inverse power law, with the power increasing monotonously with  $\eta_f$  [ 19, 24].

$R_l$  features a very strong  $M_\perp$ -dependence even without transverse flow, due to the strong longitudinal expansion of the source. It can also be described by an inverse power law, with a larger power  $\simeq 0.55$ , in rough agreement with the approximate  $\sqrt{T/M_\perp}$ -scaling law suggested in [ 25] (see, however, [ 19, 28] for a more quantitative discussion). The increase of  $R_o$  at small  $M_\perp$  is due to the contribution (63) from the effective lifetime. As seen in Fig. 5 below, in the YK frame (source rest frame) the latter is of order 2.5 fm/c at small  $M_\perp$ ; Fig. 2b shows that its effect on  $R_o$  compared to  $R_s$  in the CMS is much smaller (and thus more difficult to measure). Fig. 2d shows that the cross-term is small in the CMS but non-zero. It vanishes at  $K_\perp = 0$  by symmetry and also becomes small again at large  $K_\perp$ .

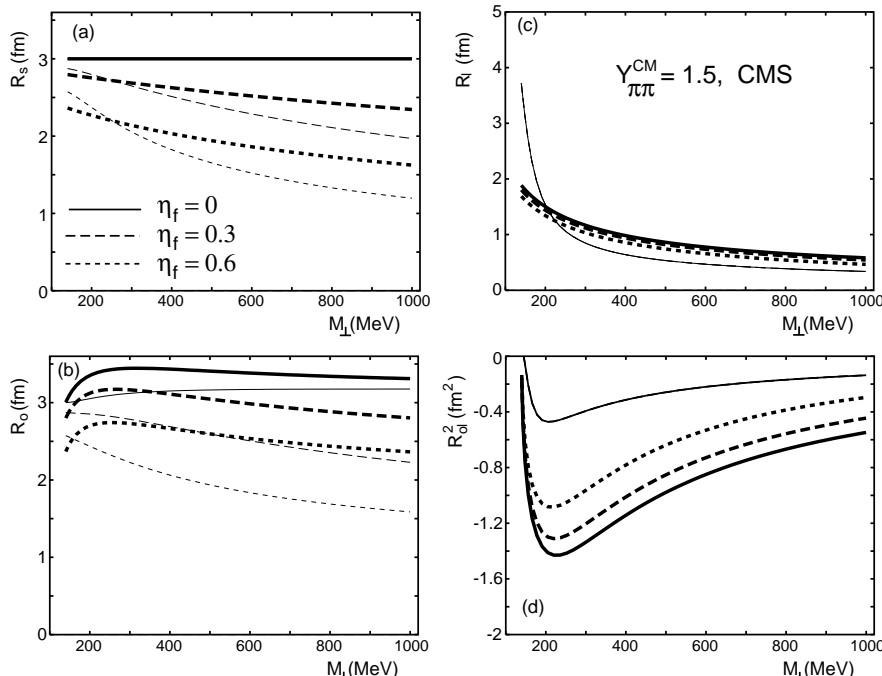


**Fig. 2.** The standard Cartesian parameters  $R_s$  (a),  $R_o$  (b),  $R_l$  (c), and  $R_{ol}^2$  (d) in the CMS for pion pairs with c.m. rapidity  $Y = 1.5$ , as functions of  $M_\perp$  for 3 different values for the transverse flow  $\eta_f$ . The thick lines are exact numerical results from Eqs. (59-62), the thin lines are obtained from the analytical approximations given in Ref. [ 22]. (Figure taken from Ref. [ 30].)

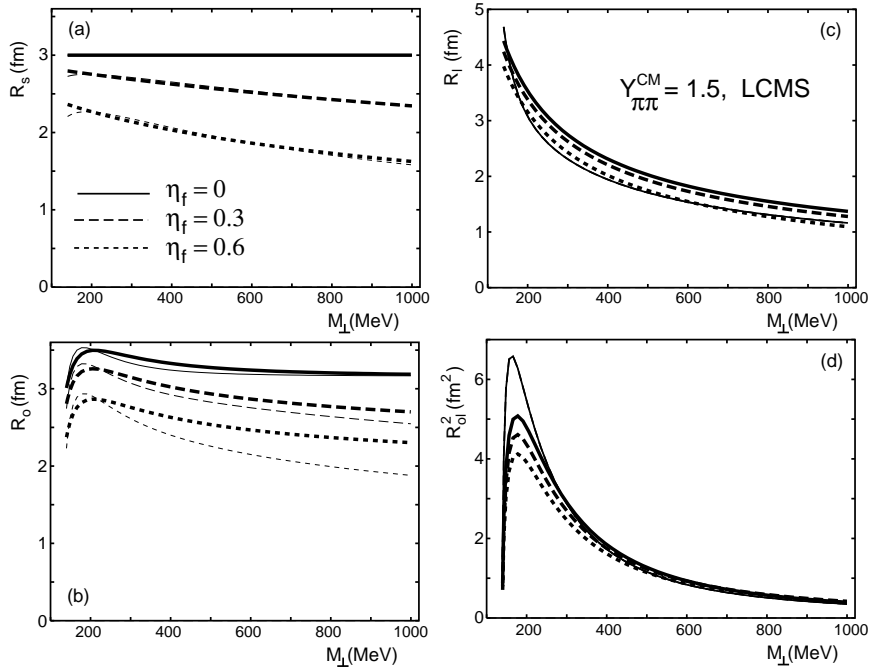
The thin lines in Fig. 2 show for comparison approximate results for the HBT radii calculated from the approximate analytical results given in Ref. [ 22] which were derived by evaluating Eqs. (59-62) by saddle point integration. It is clear that this method fails here (see Ref. [ 19] for a quantitative discussion of this approximation), and that the analytical expressions should not be used for a quantitative analysis of HBT data.

Fig. 3 shows the same situation as Fig. 2, but now all HBT radii are evaluated in the LCMS (longitudinally comoving system [ 31]) which moves with the pair rapidity

$Y = 1.5$  relative to the CMS. A comparison with Fig. 2 shows the strong reference frame dependence of the standard HBT radii. In particular, the cross-term changes sign and is now much larger. The analytical approximations from Ref. [22] work much better in the LCMS [22], but for  $R_o$  and  $R_{o\perp}^2$  they are still not accurate enough (in particular in view of the delicate nature of the lifetime effects on  $R_o$ ).

#### 4.2.3. The Yano-Koonin velocity

Fig. 4 shows (for pion pairs) the dependence of the YK velocity on the pair momentum  $\mathbf{K}$ . In Fig. 4a we show the YK rapidity  $Y_{\text{YK}} = \frac{1}{2} \ln[(1+v)/(1-v)]$  as a function of the pair rapidity  $Y$  (both relative to the CMS) for different values of  $K_{\perp}$ , in Fig. 4b the same quantity as a function of  $K_{\perp}$  for different  $Y$ . Solid lines are without transverse flow, dashed lines are for  $\eta_f = 0.6$ . For large  $K_{\perp}$  pairs, the YK rest frame approaches the LCMS (which moves with the pair rapidity  $Y$ ); in this limit all pairs are thus emitted from a small region in the source which moves with the same longitudinal velocity as the pair. For small  $K_{\perp}$  the YK frame is considerably slower than the LCMS; this is due to the thermal smearing of the particle velocities in our source



**Fig.3.** Same as Fig. 2, but now evaluated in the LCMS. Please note the change of sign and magnitude of the cross-term. (Figure taken from Ref. [30].)

around the local fluid velocity  $u^\mu(x)$  [24]. The linear relationship between the rapidity  $Y_{\text{YK}}$  of the Yano-Koonin frame and the pion pair rapidity  $Y$  is a direct reflection of the boost-invariant longitudinal expansion flow [23]. For a non-expanding source  $Y_{\text{YK}}$  would be independent of  $Y$ . Additional transverse flow is seen to have nearly no effect. The dependence of the YK velocity on the pair rapidity thus measures directly the longitudinal expansion of the source and cleanly separates it from its transverse dynamics. A detailed discussion of these features is given in Ref. [24] where it is also shown that the YK velocity is always very close to the velocity of the Longitudinal Saddle Point System LSPS (i.e. to the longitudinal velocity of the fluid element around the point of maximal emissivity at momentum  $K$ ). This last observation establishes the usefulness of the YK velocity (which can be directly extracted from an YKP fit to

the data) as a measure for the longitudinal expansion velocity of the source.

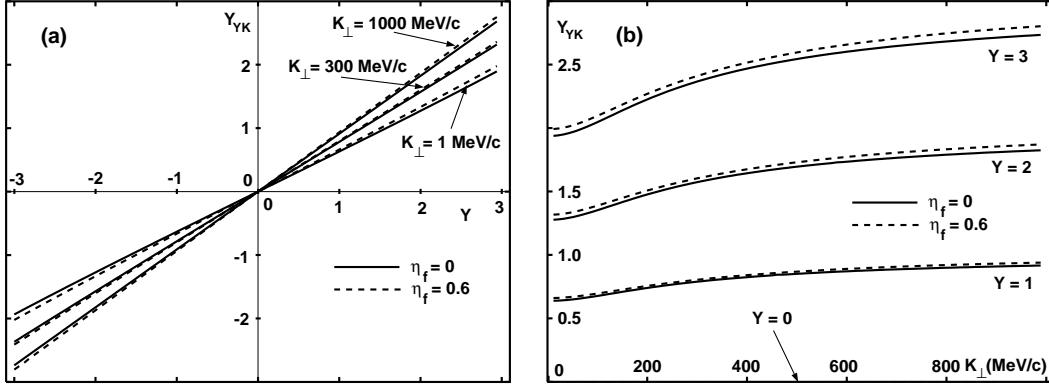


**Fig.4.** (a) The Yano-Koonin rapidity for pion pairs, as a function of the pair c.m. rapidity  $Y$ , for various values of  $K_{\perp}$  and two values for the transverse flow  $\eta_f$ . (b) The same, but plotted against  $K_{\perp}$  for various values of  $Y$  and  $\eta_f$ . (Figure taken from Ref. [ 23].)

#### 4.2.4. YKP radii: $M_{\perp}$ -scaling and transverse flow

In the absence of transverse flow, a thermal source like (80) depends on the particle rest mass and on the transverse momentum  $K_{\perp}$  only through the combination  $M_{\perp}^2 = m^2 + K_{\perp}^2$  (see Eq. (92)). Furthermore, the source is then azimuthally and  $x \rightarrow -x$  reflection symmetric. Hence  $\langle \tilde{x}\tilde{t} \rangle$ ,  $\langle \tilde{x}\tilde{z} \rangle$ , and  $\langle \tilde{x}^2 - \tilde{y}^2 \rangle$  all vanish and the approximations in Eqs. (67,68) become exact. As a result, all three YKP radii (66)-(68) are only functions of  $M_{\perp}$ , too (as well as of  $Y$ , of course), i.e. they do not depend explicitly on

the particle rest mass.

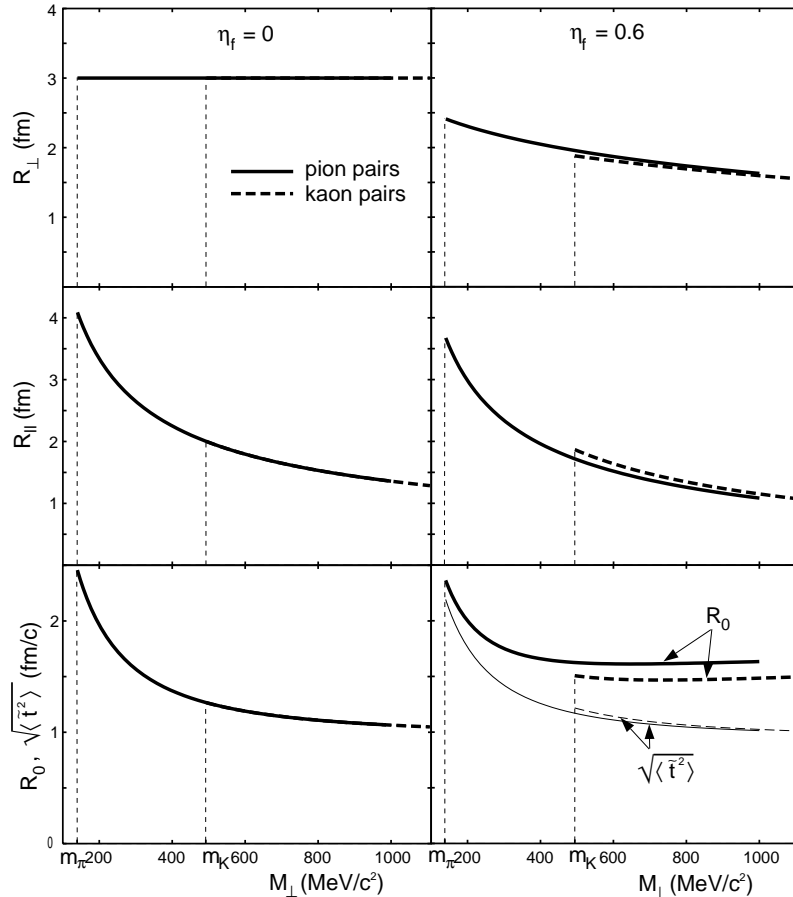


**Fig.5.** The YKP radii  $R_{\perp}$ ,  $R_{\parallel}$ , and  $R_0$  (from top to bottom) for vanishing transverse flow (left column) and for  $\eta_f = 0.6$  (right column), as functions of  $M_{\perp}$  for pairs at  $Y_{\text{cm}} = 0$ . Solid (dashed) lines are for pions (kaons). The breaking of the  $M_{\perp}$ -scaling by transverse flow is obvious in the right column. Also, as shown in the lower right panel, for nonzero transverse flow  $R_0$  does not agree exactly with the effective source lifetime  $\sqrt{\langle t^2 \rangle}$ . (Figure taken from Ref. [ 24].)

This is seen in the left column of Fig. 5 where the three YKP radii are plotted for  $Y_{\text{cm}} = 0$  pion and kaon pairs as functions of  $M_{\perp}$ ; they agree perfectly. The transverse radius here shows no  $M_{\perp}$ -dependence due to the absence of transverse temperature gradients, but even with temperature gradients it would only depend on  $M_{\perp}$ . (Of course, this discussion neglects resonance decays which will be studied in Sec. 4.3.) The very strong  $M_{\perp}$ -dependence of the longitudinal radius parameter  $R_{\parallel}$  is again due to the strong longitudinal expansion of the source. Note that  $M_{\perp}$ -scaling in the absence of transverse flow applies only to the YKP radius parameters: since the expressions (60)-(62) involve nonvanishing variances with  $\beta_{\perp}$ - or  $\beta_t$ -prefactors (which depend explicitly on the rest mass), the HBT radii from the standard Cartesian fit do not exhibit  $M_{\perp}$ -scaling.

For non-zero transverse flow  $\eta_f \neq 0$  this  $M_{\perp}$ -scaling is broken by two effects: first, the second term in (92) destroys the  $M_{\perp}$ -scaling of the emission function itself, and second the  $\beta$ -dependent correction terms in (67,68) are now non-zero because the same term also breaks, for  $K_{\perp} \neq 0$ , the  $x \rightarrow -x$  and  $x \rightarrow y$  symmetries. The magnitude of the associated scale breaking due to the pion-kaon mass difference is seen in the right column of Fig. 5 for  $\eta_f = 0.6$ . The effects are small and require very accurate experiments for their detection. However, the sign of the effect is opposite for  $R_{\parallel}$  and

for  $R_\perp, R_0$  which may help to distinguish flow-induced effects from resonance decay contributions.

Since for  $Y_{\text{cm}} = 0$  the YK and CMS frames coincide,  $\beta_l = 0$  in the YK frame and the approximation in (67) remains exact even for non-zero transverse flow. The same is not true for the approximation in (68), and therefore I show in the lower right panel of Fig. 5 also the effective source lifetime  $\sqrt{\langle \tilde{t}^2 \rangle}$  for comparison. The apparently rather large discrepancies between the YKP parameter  $R_0$  and the effective source lifetime is due to a rather extreme choice of parameters: a large flow transverse flow and a small intrinsic source lifetime of  $\Delta\tau = 1 \text{ fm}/c$  in (81). Since  $\sqrt{\langle \tilde{t}^2 \rangle}$  approaches  $\Delta\tau$  in the limit of large  $M_\perp$  while the dominant [24] correction term  $\langle \tilde{x}^2 - \tilde{y}^2 \rangle$  does not depend on  $\Delta\tau$ , the YKP parameter  $R_0$  will track the effective source lifetime more accurately for larger values of  $\Delta\tau$  (and for smaller values of  $\eta_f$ ).

Why do  $\sqrt{\langle \tilde{t}^2 \rangle}$  and  $R_0$  increase at small  $M_\perp$ ? Due to the rapid longitudinal expansion, the longitudinal region of homogeneity  $R_\parallel$  is a decreasing function  $M_\perp$ . Since for different pair momenta  $R_0$  measures the source lifetime in different YK reference frames, the freeze-out “hypersurface” will in general appear to have different shapes for pairs with different momenta. Only in our model, where freeze-out occurs at fixed proper time  $\tau_0$  (up to a Gaussian smearing with width  $\Delta\tau$ ), is it frame-independent. It is thus generally unavoidable (and here, of course, true in any frame) that freeze-out at different points  $z$  in the source will occur at different times  $t$  in the YK frame. Since a  $z$ -region of size  $R_\parallel$  contributes to the correlation function,  $R_\parallel$  determines how large a domain of this freeze-out surface (and thus how large an interval of freeze-out times in the YK frame) is sampled by the correlator. This interval of freeze-out times combines with the intrinsic Gaussian width  $\Delta\tau$  to yield the total effective duration of particle emission. It will be largest at small pair momenta where the homogeneity region  $R_\parallel$  is biggest, and will reduce to just the variance of the Gaussian proper time distribution at large pair momenta where the longitudinal (and transverse) homogeneity regions shrink to zero. The rise of  $\Delta t(\mathbf{K})$  at small  $\mathbf{K}$  is thus generic.

While the strong  $M_\perp$ -dependence of the longitudinal radius parameter  $R_\parallel$  arises from the strong longitudinal expansion, the weaker  $M_\perp$ -dependence of the transverse radius parameter reflects the weaker transverse expansion of our source. Following a suggestion by Th. Alber [48], this relation can be made quantitative: in Fig. 6 we plot in the left column the transverse and longitudinal YKP radii  $R_\perp$  and  $R_\parallel$  versus  $M_\perp$  on a double-logarithmic scale. We see that both can be approximately represented by power laws. (The same is not true for  $R_0$ .) While in such a plot the slope of  $R_\perp$  clearly increases with the strength  $\eta_f$  of the transverse flow, the slope of  $R_\parallel$  appears to be insensitive to transverse flow. This can be seen quantitatively in the right column of Fig. 6 where we plot the powers  $\alpha_\perp, \alpha_\parallel$  extracted from a fit

$$R_\perp(M_\perp) \propto M_\perp^{-\alpha_\perp}, \quad R_\parallel(M_\perp) \propto M_\perp^{-\alpha_\parallel} \quad (102)$$

as a function of  $\eta_f$ . As indicated in Fig. 6b the extracted power  $\alpha_\perp$  for  $R_\perp$  depends somewhat on the fit region because  $R_\perp$  doesn't follow an exact power law; independent of the fit region it increases, however, monotonously and nearly linearly with the strength  $\eta_f$  of the transverse flow. Kaons “feel” the transverse flow more strongly than pions, as reflected by the somewhat larger powers  $\alpha_\perp$  at fixed  $\eta_f$ . Note that even for a rather strong transverse flow  $\eta_f = 0.6$  (heavy-ion data seem to require less flow)  $\alpha_\perp$

remains below 0.25.

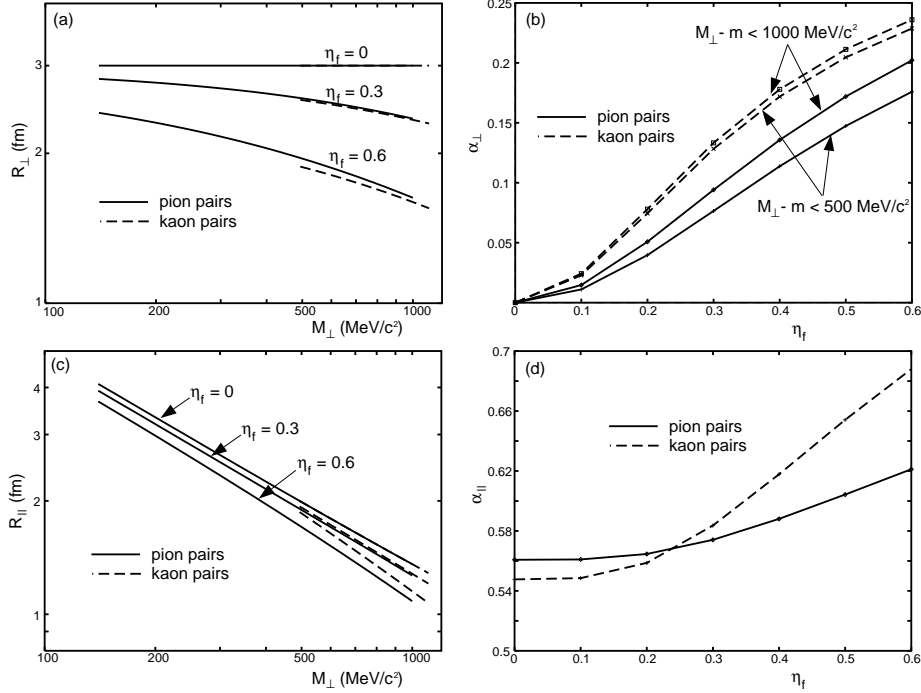


**Fig. 6.** (a)  $R_{\perp}$  as a function of  $M_{\perp}$  at  $Y_{\text{CM}} = 0$ , for pions (solid) and kaons (dashed) and different transverse flow rapidities  $\eta_f$ . (b) The scaling coefficient  $\alpha_{\perp}$  defined by  $R_{\perp} \approx M_{\perp}^{-\alpha_{\perp}}$  for pions (solid) and kaons (dashed) as a function of the transverse flow rapidity  $\eta_f$ . The different results obtained by fitting in the regions  $M_{\perp} - m < 500$  MeV/ $c^2$  and  $M_{\perp} - m < 1000$  MeV/ $c^2$  are shown separately. (c) Same as (a), but for  $R_{\parallel}$ . (d) Same as (b), but for  $\alpha_{\parallel}$ . (Figure taken from Ref. [ 24].)

The power  $\alpha_{\parallel}$  for  $R_{\parallel}$  is shown in Fig. 6d. It has a much larger value of 0.55-0.56 even for  $\eta_f = 0$ , reflecting the strong boost-invariant longitudinal expansion. As  $\eta_f$  increases,  $\alpha_{\parallel}$  also increases, but only by a few percent. (Note the suppressed zero in Fig. 6d!) Again, kaons are affected more strongly by the transverse flow than pions, but altogether the  $M_{\perp}$ -dependence of  $R_{\parallel}$  is rather insensitive to transverse flow.

As observed by Th. Alber in his thesis [ 48] these features agree qualitatively with the heavy-ion data: for  $\alpha_{\parallel}$  he found values of order 0.4–0.5, while  $\alpha_{\perp}$  remained smaller, of order 0.1–0.2; in  $^{32}\text{S}$ -induced collisions, the central values for both numbers showed a systematic tendency to increase with the mass of the target nucleus, indicating stronger collective flow in larger collision systems than in smaller ones. The error bars on the  $\alpha$ 's were, however, large, and one should wait for independent confirmation before firmly drawing such a conclusion.

The  $Y$ -dependence of the Yano-Koonin rapidity  $Y_{\text{YK}}$  and the  $M_{\perp}$ -dependence of  $R_{\parallel}$  can thus be used as a quantitative measure for the longitudinal expansion of the source which is hardly affected at all by the presence and strength of transverse flow. On the other side,  $R_{\perp}$  being boost-invariant, the  $M_{\perp}$ -dependence of  $R_{\perp}$  is independent of the longitudinal expansion of the source and reflects only its transverse expansion. Together with the breaking of the  $M_{\perp}$ -scaling of the YKP radii, the  $M_{\perp}$ -dependence of  $R_{\perp}$  can thus be used to extract quantitatively the transverse expansion velocity of the source [ 46, 24].

### 4.3. Resonance decays

As already mentioned pions in particular have the problem that in high-energy collisions only a fraction of about 50% or less of all pions come directly from the decoupling source while the rest are produced after decoupling by the decay of unstable resonances. The above considerations presuppose that the resonance decays do not affect the  $M_{\perp}$ -dependence of  $R_{\perp}$ . This is not obvious, in particular since it is known that the  $M_{\perp}$ -dependence of the single-pion spectrum is very strongly affected by resonance decays [ 49]. Since resonance decays contribute more to pions than to kaons they may also affect the  $M_{\perp}$ -scaling arguments. The work by the Marburg group [ 40] on resonance decay effects on HBT in the context of hydrodynamical simulations indicates, within the standard Cartesian framework and without accounting for the cross-term, a possible additional  $M_{\perp}$ -dependence of the transverse radius. However, a systematic analysis of resonance contributions to HBT as a function of various characteristic source parameters is only now becoming available [ 50, 51].

#### 4.3.1. Formalism

Not much is known directly from experiment about the amount of resonance production in heavy-ion collisions. For  $pp$  collisions at similar energies a thermal model, where resonances are produced with thermal abundances in mutual chemical equilibrium, appears to work surprisingly well [ 52, 49, 53]. We therefore assume the same to hold for heavy-ion collisions. We also assume for simplicity that all hadrons decouple at the same point. Thus all resonances are assumed to have the same emission function (80-82), adjusted only for the particle rest mass  $m_i$ , its spin  $J_i$ , and its chemical potential  $\mu_i$ . In chemical equilibrium  $\mu_i$  is given in terms of the two independent chemical potentials  $\mu_b$  and  $\mu_s$  which account for conservation of baryon number and strangeness:

$$\mu_i = b_i \mu_b + s_i \mu_s, \quad (103)$$

where  $b_i, s_i$  are the baryon number and strangeness for resonance species  $i$ .  $\mu_s$  is determined in terms of  $T$  and  $\mu_b$  by the condition of strangeness neutrality of the collision region [ 54] which cannot be violated on the time scale of strong interactions. For illustration we will below consider the case  $\mu_b = \mu_s = 0$ .

I will now describe very shortly the formal steps for calculating the resonance contributions to the correlation function; for more details I refer the reader to Ref. [ 50]. The total source distribution of pions (and similarly for other stable particle species, although for pions the resonance contributions are most important) can be written as

$$S_{\pi}(x, p) = S_{\pi}^{\text{dir}}(x, p) + \sum_{r \neq \pi} S_{r \rightarrow \pi}(x, p), \quad (104)$$

where the first term on the r.h.s. is the contribution from the directly emitted pions (Eq. (80) with  $J = 0, m = m_{\pi}$ ) and the sum contains all contributions from resonance feed-down:

$$\begin{aligned} S_{r \rightarrow \pi}(x, p) &= M_r \int_{s_-}^{s_+} ds g(s) \int \frac{d^3 P}{E_P} \delta(p \cdot P - M_r E^*) \\ &\times \int d^4 X \int_0^{\infty} d\tau \Gamma e^{-\Gamma \tau} \delta^{(4)} \left( x - \left( X - \frac{P}{M_r} \tau \right) \right) S_r^{\text{dir}}(X, P). \end{aligned} \quad (105)$$

Here capital letters indicate coordinates associated with the parent resonance  $r$ , lower case letters are associated with the decay pion.  $s$  is the the invariant mass of the other, unobserved decay products; in an  $n$ -body decay, it can vary between  $s_- = (\sum_{i=2}^n m_i)^2$

and  $s_+ = (M_r - m_\pi)^2$ .  $g(s)$  is the decay phase space for the  $(n-1)$  unobserved particles; for the isotropic 2-body decay of an unpolarized resonance it is given by

$$g(s) = \frac{b_{r \rightarrow \pi}}{4\pi p^*} \delta(s - m_2^2), \quad (106)$$

(where  $b_{r \rightarrow \pi}$  is the branching ratio for the decay channel), and for isotropic 3-body decays by [ 55]

$$g(s) = \frac{M_r b_{r \rightarrow \pi}}{2\pi s} \frac{\sqrt{[s - (m_2 + m_3)^2][s - (m_2 - m_3)^2]}}{Q(M_r, m_\pi, m_2, m_3)}, \quad (107)$$

$$Q(M_r, m_\pi, m_2, m_3) = \int_{s_-}^{s_+} \frac{ds'}{s'} \sqrt{(M_r + m_\pi)^2 - s'} \sqrt{s_+ - s'}$$

$$\times \sqrt{s_- - s'} \sqrt{(m_2 - m_3)^2 - s'}.$$

$p^*, E^*$  are the momentum and energy of the decay pion in the resonance rest frame,

$$E^* = \sqrt{m_\pi^2 + p^{*2}}, \quad p^* = \frac{\sqrt{[(M_r + m_\pi)^2 - s][(M_r - m_\pi)^2 - s]}}{2M_r}, \quad (108)$$

and functions of  $s$  only. The  $\tau$ -integration in (105) extends over the exponential decay probability of the resonance with total decay width  $\Gamma$ . The 4-dimensional  $\delta$ -function of the space-time coordinate  $X$  ensures that for the pion to appear at point  $x$  from a resonance decaying at time  $\tau$ , the parent resonance with momentum  $P$  must have been emitted from the source at point  $X - (P/M_r)\tau$ .

The integration over the resonance momentum  $P$  is restricted by the energy-momentum constraint  $\delta(p \cdot P - M_r E^*)$ . In the coordinate system where the momentum  $p$  of the decay pion is given by

$$p^\mu = (m_\perp \cosh y, p_\perp, 0, m_\perp \sinh y), \quad (109)$$

(see (89)), the resonance momentum  $P$  is parametrized as

$$P^\mu = (M_\perp \cosh Y, P_\perp \cos \Phi, P_\perp \sin \Phi, M_\perp \sinh Y). \quad (110)$$

For  $p_\perp \neq 0$  the  $\delta$ -function can be used to fix the azimuthal angle  $\Phi$  of the resonance momentum  $P$  to

$$\Phi_\pm = \pm \tilde{\Phi} \quad \text{with} \quad \cos \tilde{\Phi} = \frac{E E_P - p_\perp P_\perp - E^* M}{p_\perp P_\perp} = \frac{m_\perp M_\perp \cosh(Y - y) - E^* M}{p_\perp P_\perp}. \quad (111)$$

Let us denote by  $P^\pm$  the two values of  $P$  obtained by inserting the two solutions (111) into (110). After doing the  $\Phi$ - and  $X$ -integrations in (105) one thus obtains

$$S_{r \rightarrow \pi}(x, p) = M_r \int_{s_-}^{s_+} ds g(s) \int_{Y_-}^{Y_+} dY \int_{M_{\perp,-}^2}^{M_{\perp,+}^2} dM_\perp^2 \int_0^\infty d\tau \Gamma e^{-\Gamma\tau}$$

$$\times \frac{\frac{1}{2} \sum_\pm S_r^{\text{dir}} \left( x - \frac{P^\pm}{M_r} \tau, P^\pm \right)}{\sqrt{p_\perp^2 (M_\perp^2 - M_r^2) - [E^* M_r - m_\perp M_\perp \cosh(Y - y)]^2}}, \quad (112)$$

with the kinematic limits

$$M_{\perp,\pm} = \overline{M}_\perp \pm \Delta M_\perp \quad (113)$$

$$\equiv \frac{E^* M_r m_\perp \cosh(Y - y)}{m_\perp^2 \cosh^2(Y - y) - p_\perp^2} \pm \frac{M_r p_\perp \sqrt{E^{*2} + p_\perp^2 - m_\perp^2} \cosh^2(Y - y)}{m_\perp^2 \cosh^2(Y - y) - p_\perp^2}$$

$$Y_\pm = y \pm \Delta Y \equiv y \pm \ln \left( \frac{p^*}{m_\perp} + \sqrt{1 + \frac{p^{*2}}{m_\perp^2}} \right) \quad (114)$$

resulting from the zeroes of the square root in the denominator (which, incidentally, can also be written as  $p_\perp P_\perp |\sin \tilde{\Phi}|$ ). – For the limiting case  $p_\perp = 0$ , the constraint  $p \cdot P = M_r E^*$  cannot be used to do the  $\Phi$ -integration. One then uses it to do the  $M_\perp$ -integral:

$$S_{r \rightarrow \pi}(x; y, p_\perp = 0) = M_r \int_{s_-}^{s_+} ds g(s) \int_0^\pi d\Phi \int_{Y_-}^{Y_+} dY \frac{M_r E^*}{m^2 \cosh^2(Y - y)} \\ \times \int d\tau \Gamma e^{-\Gamma\tau} S_r^{\text{dir}} \left( x - \frac{P}{M_r} \tau, P \right) \Big|_{M_\perp = \frac{M_r E^*}{m_\pi \cosh(Y-y)}}. \quad (115)$$

For the more generic case  $p_\perp \neq 0$  a few further manipulations are useful in practice [ 50]: Rewriting the square root in (112) as

$$\frac{1}{\sqrt{m_\perp^2 \cosh^2(Y - y) - p_\perp^2}} \frac{1}{\sqrt{(\Delta M_\perp)^2 - (M_\perp - \bar{M}_\perp)^2}} \quad (116)$$

and introducing new integration variables  $v \in [-1, 1]$ ,  $\zeta \in [-\pi, \pi]$  via

$$M_\perp = \bar{M}_\perp + \Delta M_\perp \cos \zeta, \quad (117)$$

$$Y = y + v \Delta Y, \quad (118)$$

Eq. (112) can be further transformed into

$$S_{R \rightarrow \pi}(x, p) = \sum_{\pm} \int_{\mathbf{R}} \int_0^\infty d\tau \Gamma e^{-\Gamma\tau} S_R^{\text{dir}} \left( x - \frac{P^\pm}{M} \tau, P^\pm \right), \quad (119)$$

with the following shorthand for the integration over the resonance momenta:

$$\int_{\mathbf{R}} \equiv M_r \int_{s_-}^{s_+} ds g(s) \int_{-1}^1 \frac{\Delta Y dv}{\sqrt{m_\perp^2 \cosh^2(v \Delta Y) - p_\perp^2}} \int_0^\pi d\zeta (\bar{M}_\perp + \Delta M_\perp \cos \zeta). \quad (120)$$

For the calculation of the correlation function we need the Fourier transform of the emission function

$$\tilde{S}_{r \rightarrow \pi}(q, p) = \int d^4x e^{iq \cdot x} S_{r \rightarrow \pi}(x, p) = \sum_{\pm} \int_{\mathbf{R}} \frac{1}{1 - i \frac{q \cdot P^\pm}{M_r \Gamma}} \tilde{S}_r^{\text{dir}}(q, P^\pm), \quad (121)$$

and must evaluate

$$C(\mathbf{q}, \mathbf{K}) = 1 + \frac{|\tilde{S}_\pi^{\text{dir}}(q, K)|^2 + 2 \sum_{r \neq \pi} \text{Re} [\tilde{S}_\pi^{\text{dir}}(q, K) \tilde{S}_{r \rightarrow \pi}(q, K)] + |\sum_{r \neq \pi} \tilde{S}_{r \rightarrow \pi}(q, K)|^2}{|\tilde{S}_\pi(0, K)|^2}, \quad (122)$$

where the denominator includes all contributions. Numerically, this is a rather involved expression. If the resonance contributions are small compared to the direct term one can use the Grassberger approximation [ 56] in which the last term in the numerator is neglected. For heavy-ion collisions this is not good enough since about 50% of all pions come from resonance decays. Instead, we can try to exploit the connection from Lecture 2 between the half-widths of the correlation function and the space-time variances which are now given by

$$\langle \tilde{x}_\mu \tilde{x}_\nu \rangle(\mathbf{K}) = \frac{\sum_r \int d^4x \tilde{x}_\mu \tilde{x}_\nu S_{r \rightarrow \pi}(x, K)}{\sum_r \int d^4x S_{r \rightarrow \pi}(x, K)}. \quad (123)$$

Here the sum now runs over all contributions, including the direct pions. It is instructive to rewrite the average over the emission function in the following form:

$$\begin{aligned}\langle x_\nu \rangle(\mathbf{K}) &= \sum_r f_r(\mathbf{K}) \langle x_\nu \rangle_r(\mathbf{K}), \\ \langle x_\mu x_\nu \rangle(\mathbf{K}) &= \sum_r f_r(\mathbf{K}) \langle x_\mu x_\nu \rangle_r(\mathbf{K}).\end{aligned}\quad (124)$$

Here we introduced the single-particle fractions [ 40]

$$f_r(\mathbf{K}) = \frac{\int d^4x S_{r \rightarrow \pi}(x, K)}{\sum_r \int d^4x S_{r \rightarrow \pi}(x, K)} = \frac{dN_\pi^r/d^3K}{dN_\pi^{\text{tot}}}, \quad \sum_r f_r(\mathbf{K}) = 1, \quad (125)$$

which give the fraction of single pions with momentum  $\mathbf{K}$  resulting from decay channel  $r$ , and the average  $\langle \dots \rangle_r$  with the effective pion emission function arising from this particular channel:

$$\langle \dots \rangle_r(\mathbf{K}) = \frac{\int d^4x \dots S_{r \rightarrow \pi}(x, K)}{\int d^4x S_{r \rightarrow \pi}(x, K)}. \quad (126)$$

The variances (123) can then be rewritten as

$$\langle \tilde{x}_\mu \tilde{x}_\nu \rangle = \sum_r f_r \langle \tilde{x}_\mu \tilde{x}_\nu \rangle_r + \sum_{r, r'} f_r (\delta_{r, r'} - f_{r'}) \langle x_\mu \rangle_r \langle x_\nu \rangle_{r'}. \quad (127)$$

The first term has an easy intuitive interpretation: each resonance decay channel  $r$  contributes an effective emission function  $S_{r \rightarrow \pi}$ . The full variance is calculated by weighting the variance (homogeneity length) of the emission function from a particular decay channel with the fraction  $f_r$  with which this channel contributes to the single particle spectrum. The second term in (127) is due to the fact that in general the effective emission functions from the various decay channels have different saddle points; it somewhat spoils the intuitive interpretation of (123).

#### 4.3.2. Influence on HBT radii and non-Gaussian features

It turns out that, contrary to the situations discussed before, in the case of long-lived resonances the expressions (123) are not very useful for a quantitative understanding of the correlator, although certain qualitative features can still be extracted relatively easily. The reason for this is best explained by considering the simple example of only one longlived resonance in a 1-dimensional space. Let us model the emission function for the direct pions by a Gaussian in coordinate space with width  $R_{\text{dir}}$  and (somewhat unrealistically) the emission function of the pions from the decaying resonance by a second Gaussian with much larger radius  $R_{\text{halo}}$  (assuming that the resonance travels on average a distance of order  $R_{\text{halo}}$  before it decays), with weights  $\varepsilon$  and  $(1 - \varepsilon)$ , respectively:

$$S_\pi(x, K) = S_\pi^{\text{dir}}(x, K) + S_{r \rightarrow \pi}(x, K) = (1 - \varepsilon) e^{-x^2/(2R_{\text{dir}}^2)} + \varepsilon e^{-x^2/(2R_{\text{halo}}^2)}. \quad (128)$$

Then the correlator is given by

$$C(q, K) - 1 = (1 - \varepsilon)^2 e^{-R_{\text{dir}}^2 q^2} + \varepsilon^2 e^{-R_{\text{halo}}^2 q^2} + 2\varepsilon(1 - \varepsilon) e^{-(R_{\text{dir}}^2 + R_{\text{halo}}^2)q^2/2}. \quad (129)$$

If  $\varepsilon$  is small, but  $R_{\text{halo}}$  is large, then the correlator is a superposition of a large, broad Gaussian with width  $1/R_{\text{dir}}$  and weight  $(1 - \varepsilon)^2$ , a second, narrower Gaussian with width  $\sqrt{2/(R_{\text{dir}}^2 + R_{\text{halo}}^2)}$  and smaller weight  $2\varepsilon(1 - \varepsilon)$ , and a third, extremely narrow

Gaussian with width  $1/R_{\text{halo}}$  and tiny weight  $\varepsilon^2$ . Obviously, the rough structure of the correlator will be determined by the large and broad direct contribution; the two other contributions will, however, modify its functional form:

(i) If the resonance is shortlived such that  $R_{\text{halo}} \gtrsim R_{\text{dir}}$  its effect on the correlator will be minor; its shape will remain roughly Gaussian, with a width somewhere between  $1/R_{\text{dir}}$  and  $1/R_{\text{halo}}$ , depending on the weight  $\varepsilon$  of the resonance contribution.

(ii) If the resonance lifetime and thus  $R_{\text{halo}}$  are extremely large, the second and third term in (129) will be very narrow and, due to the finite two-track resolution of every experiment, may escape detection; then the correlator looks again Gaussian with a width  $1/R_{\text{dir}}$ , but at  $q = 0$  it will not approach the value 2, but  $1 + (1 - \varepsilon)^2 < 2$ . The correlation appears to be incomplete, with an ‘‘chaoticity parameter’’  $\lambda = (1 - f_r)^2 = (1 - \varepsilon)^2$ .

(iii) If the resonance lifetime is in between such that  $R_{\text{halo}} \gg R_{\text{dir}}$  but  $1/R_{\text{halo}}$  being still large enough to be experimentally resolved, all three Gaussians contribute, and the full correlator deviates strongly from a single Gaussian.

In cases (ii) and (iii) the space-time variances give misleading or outright wrong results for the width of the correlation function. As noted in connection with Eq. (53), they reproduce the curvature of the correlator at  $q = 0$  which for our toy model is

$$\frac{1}{2} \left. \frac{\partial^2 C(q)}{\partial q^2} \right|_{q=0} = (1 - \varepsilon)R_{\text{dir}}^2 + \varepsilon R_{\text{halo}}^2. \quad (130)$$

In case (ii), for not too small values of  $\varepsilon$ , this is dominated by the second term although the resonance contribution is not even visible in the correlator! On a quantitative level, the situation is not very much better for case (iii).

For the case (ii) of very long-lived resonances there is, of course, an easy way to save the usefulness of the space-time variances: if one simply leaves them out from the sum over resonances in (127), but only includes them via an ‘‘chaoticity parameter’’

$$\lambda(\mathbf{K}) = \left( 1 - \sum_{r=\text{longlived}} f_r(\mathbf{K}) \right)^2, \quad (131)$$

the roughly Gaussian contributions to the correlator from the direct pions and short-lived resonances are still correctly reproduced. The real head ache comes from resonances with an intermediate lifetime which lead to a large halo but can still be experimentally resolved. They cause appreciable deviations from a Gaussian behaviour for the correlator and cannot be reliably treated by the method of space-time variances.

In nature there is only one such resonance: the  $\omega$  meson, with a lifetime of approximately 20 fm/c. All other resonances either live so shortly (typically 1 fm/c) that they hardly modify the correlator, or so long that their contribution to the correlator cannot be resolved such that they only affect  $\lambda$ . At low  $K_{\perp}$ , however, up to 10% of all pions come from  $\omega$ -decays ( $f_{\omega}(\mathbf{K} = 0) \approx 0.1$ ), and their non-Gaussian effects on the correlator can be clearly seen. On account of the  $\omega$  a full numerical evaluation of the correlator (122) or a treatment with more powerful analytical methods which can deal with the non-Gaussian features of the correlator ( $q$ -variances, see Ref. [ 50]) become indispensable.

#### 4.3.3. $K$ -dependence of correlator including resonance decays

I now show some numerical results for the correlation functions resulting from the emission function (80), but now including the resonance contributions. The complete

spectrum of relevant resonances is included, and in the decays the 2- and 3-body decay kinematics is fully taken into account. The HBT radii are extracted from a Gaussian fit to the numerically calculated correlation function. A detailed technical discussion is given in Ref. [ 50].

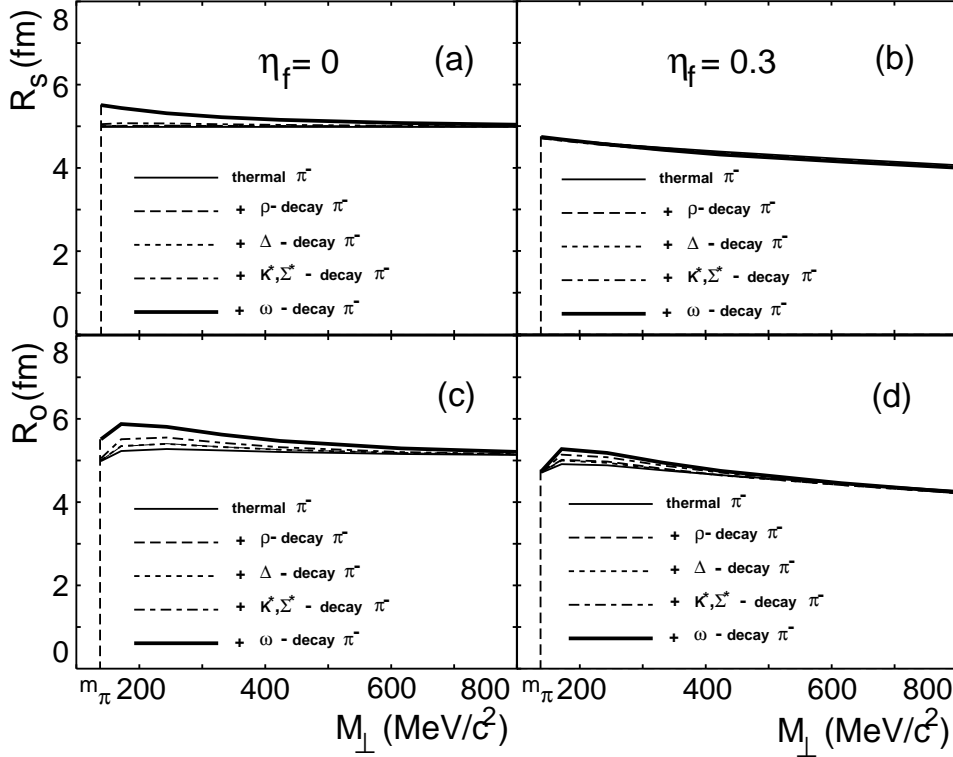


**Fig.7.** The influence of resonance decays on the  $M_{\perp}$ -dependence of  $R_s$  (a,b) and  $R_o$  (c,d) for  $Y_{\text{cm}} = 0$  pion pairs. a,c: no transverse flow; b,d: transverse flow rapidity  $\eta_f = 0.3$ . The Gaussian transverse radius is here  $R = 5$  fm, and  $T = 150$  MeV. The HBT radii are extracted from unidirectional fits to the correlator in the respective direction of  $\mathbf{q}$ . (Figure taken from Ref. [ 50].)

Fig. 7 shows results for the standard Cartesian parameters  $R_s$  and  $R_o$  from 1-dimensional fits to the numerically computed correlator in the respective ( $q_s$  or  $q_o$ ) directions (setting the other components of  $\mathbf{q}$  to zero). One sees that the effects of the short-lived resonances with lifetimes of order 1 fm/c on  $R_s$  are essentially negligible, both at vanishing and at nonzero transverse flow. Only the  $\omega$  with its intermediate lifetime of 20 fm/c affects  $R_s$ , but only for vanishing transverse flow. There it induces a weak  $M_{\perp}$ -dependence at small  $M_{\perp}$  even in the absence of transverse flow; at  $M_{\perp} > 500$  MeV the contribution of the  $\omega$  dies out, and  $R_s$  again becomes  $M_{\perp}$ -independent (which would not be the case if it were affected by flow). At  $\eta_f = 0.3$  and 0.6 [ 50] not even the  $\omega$  generates any additional  $M_{\perp}$ -dependence!  $-R_o$  shows some effects from the additional lifetime of the resonances, in particular from the long-lived  $\omega$ . Resonances with much longer lifetimes than the  $\omega$  (in particular all weak decays) cannot be resolved

experimentally in the correlator and have no effect on the HBT radii.

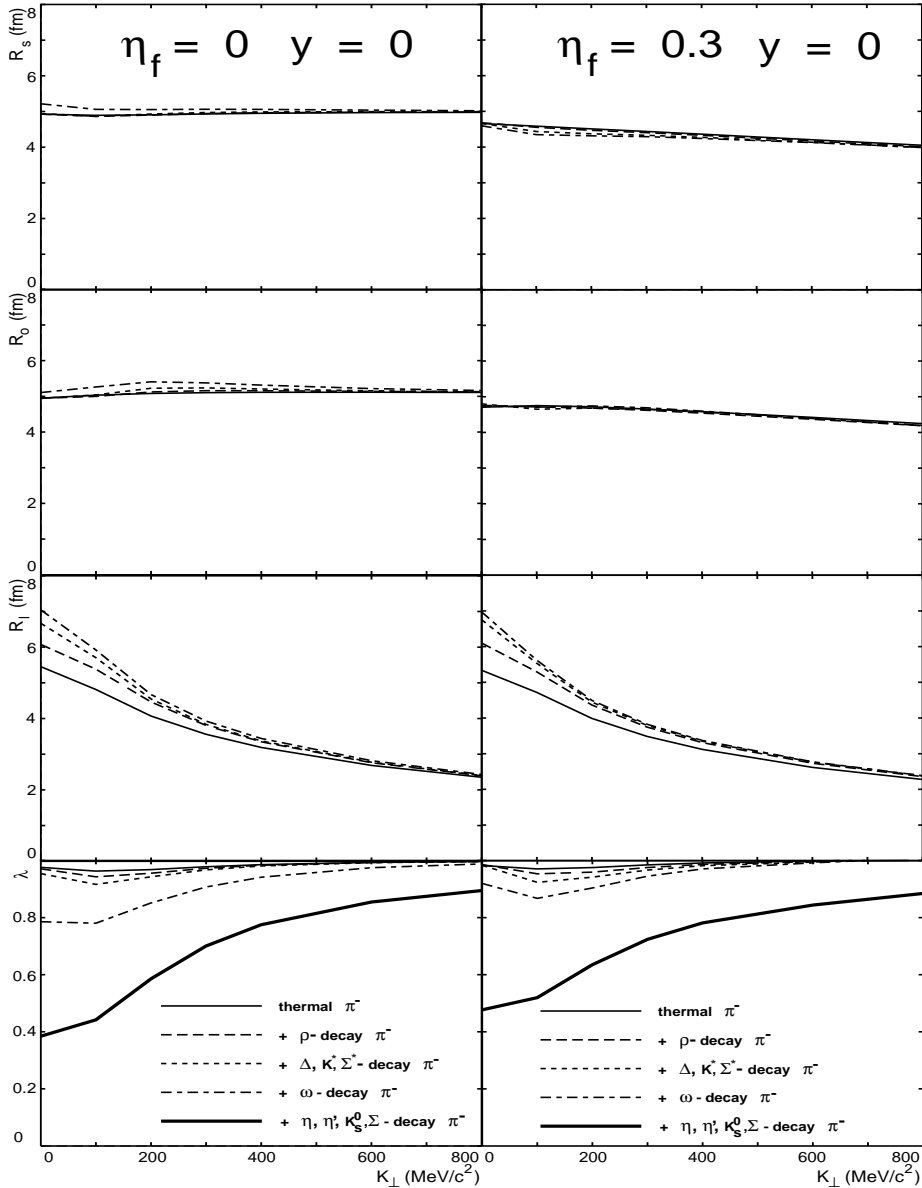


**Fig.8.** Same as Fig. 7, but now with parameters extracted from a complete 5-dimensional fit to the correlator (see text). Top row:  $R_s$ ; second row:  $R_o$ ; third row:  $R_l$ ; bottom row: effective chaoticity parameter  $\lambda$ . Left column: no transverse flow; right column: transverse expansion with  $\eta_f = 0.3$ . The cross term  $R_{ol}$  vanishes for  $Y = 0$  pairs. (Figure taken from Ref. [ 50].)

The weak effect of resonances on  $R_s = R_\perp$  seems surprising: due to their non-zero lifetime they should be able to propagate outside the original source before decay and form a pion “halo” [ 40, 57]. This effect is, however, much weaker than naively expected: most of the resonances are not very fast, and the halo thickness is thus only a fraction of the resonance lifetime. At finite transverse flow an additional effect comes into play: it turns out that then the effective size of the emission function for directly emitted resonances is *smaller* than that for direct pions [ 50]! At  $\eta_f=0.3$  and 0.6 this even slightly overcompensates the halo effect, and altogether the resonances change neither the size nor the  $M_\perp$ -dependence of  $R_s$ .

In Fig. 8 also the longitudinal radius  $R_l$  is shown. Here even the shortlived resonances are seen to make an effect. It can be essentially traced to a lifetime effect: Since the pions from the short-lived resonances appear typically 1 fm/c later than the direct

pions, the source has in the meantime expanded longitudinally to a situation with a smaller longitudinal velocity gradient (the latter goes like  $1/\tau$ ). Thus the resulting pion source has a larger longitudinal length of homogeneity and features a larger value  $R_l$ .

#### 4.3.4. The “chaoticity parameter” $\lambda$

As noted above, the  $\omega$ -decays make the correlator non-Gaussian. Slight non-Gaussian features exist even without resonance decays in the longitudinal direction, induced by the strong longitudinal flow, and for large transverse flow  $\eta_f$  become also visible in the transverse direction. A Gaussian fit to such a slightly non-Gaussian correlator in general does not extrapolate to the correct value at  $\mathbf{q} = 0$ , but introduces an effective “chaoticity parameter”  $\lambda$ . In 1-dimensional fits along the three cartesian directions of  $\mathbf{q}$  the different degrees of non-Gaussianity lead to different values of  $\lambda$ . This situation is aggravated by the resonance contributions, in particular from the  $\omega$  which affects the correlator differently in each direction. Still a different value of  $\lambda$  is found in a 5-dimensional fit to the correlator, using the 4 standard Cartesian HBT radii and  $\lambda$  as fit parameters, because now  $\lambda$  has to “compromise” between the values found in the unidirectional fits. From the last row in Figs. 8 one sees that even without the contribution from the  $\omega$  and the longlived resonances the effective  $\lambda$  is below 1 by up to 10%; inclusion of the  $\omega$  reduces it further to about 80-85% at  $\mathbf{K} = 0$ . Thus not only the very longlived resonances affect  $\lambda$  as anticipated above, but so do to some extent the medium- and shortlived resonances and even flow.

Comparing Figs. 7 and Fig. 8 one sees that this compromise in  $\lambda$  between the 3 different unidirectional fit values and the one resulting in the 5-dimensional fit also changes the fitted HBT radii. On the same (small) level as already observed for the contribution from  $\omega$  decays, it even affects the  $M_\perp$ -dependence of  $R_\perp$ . Both effects, the non-Gaussian features of the correlator and the effective “chaoticity parameter” which differs from  $\lambda = 1$ , vanish at large  $\mathbf{K}$  because the resonance decay pions are concentrated at low  $\mathbf{K}$  [ 49].

## 5. FINAL REMARKS

In these three lectures I have presented to you two-particle intensity interferometry for relativistic heavy-ion collisions both as an intellectually stimulating problem and as a powerful practical method. Its application to nuclear collisions has turned out to be much more difficult than expected from the astrophysical analogue (two-photon intensity interferometry of stars). But at the same time, due to the dynamical nature of the problem, the physics of heavy-ion collisions is very much richer, and I have tried to show you that the HBT method is up to the task of clarifying a lot of this physics in a rather direct manner.

The key to our understanding of the HBT method and how to apply it to dynamical situations are the model-independent expressions derived in the second lecture, which express the HBT width parameters in terms of second order space-time variances of the emission function. They provide the basis of a detailed physical interpretation of the measured HBT radii. They show that generally the HBT radius parameters do not measure the full geometric extension of the source, but regions of homogeneity inside the effective emission function for particles with certain fixed momenta. For expanding systems these are usually smaller than the naive geometric source size and decreasing functions of the pair momentum. For systems with finite lifetime the HBT parameters usually mix the spatial and temporal structure of the source, and their

unfolding requires model studies.

With the new YKP parametrization a method has been found which, for systems with dominant longitudinal expansion, cleanly factorises the longitudinal and transverse spatial from the temporal homogeneity length. The effective source lifetime is directly fitted by the parameter  $R_0$ ; it is generically a function of the pair momentum and largest for pairs which are slow in the CMS. Another fit parameter, the YK velocity, measures directly the longitudinal velocity of the emitting fluid element, and its dependence on the pair rapidity allows for a direct determination of the longitudinal expansion of the source. Without transverse expansion, the YKP radius parameters show exact  $M_\perp$ -scaling. The breaking of this scaling and the  $M_\perp$ -dependence of the transverse radius parameter  $R_\perp$  allow for a determination of the transverse expansion velocity of the source. Resonance decays were shown to mostly affect the lifetime parameter and, as a consequence, the longitudinal homogeneity length. They leave the  $M_\perp$ -dependence of  $R_\perp$  nearly unchanged and thus do not endanger the extraction of the transverse flow via HBT.

With this new and detailed understanding of the method, I believe that HBT interferometry has begun a new and vigorous life as a powerful tool for reconstructing the geometric and dynamic space-time characteristics of the collision zone from the measured momentum spectra.

**Acknowledgements:** I wish to express my thanks to my collaborators on this project, S. Chapman, J.R. Nix, B. Tomášik, U.A. Wiedemann, and Wu Yuanfang, who each contributed valuable pieces to the results presented in these lectures. Working with them has always been a pleasure. I would also like to acknowledge stimulating discussions with H. Appelshäuser, T. Csörgő, D. Ferenc, M. Gaździcki, B. Jacak, and P. Seyboth. Last but not least I would like to thank the organizers of this summer school for the invitation to come here and the students for their enthusiasm and for a pleasant and entertaining week in Dronten with many interesting conversations. This work was supported by grants from BMBF, DFG, and GSI.

## References

- [1] J. Schukraft, lecture notes in this volume.
- [2] D. Boal, C.K. Gelbke, and B. Jennings, *Rev. Mod. Phys.* **62** (1990) 553.
- [3] B. Jacak, lecture notes in this volume.
- [4] *Quark Matter '96*, edited by P. Braun-Munzinger et al., *Nucl. Phys. A* (1996), in press.
- [5] M. Gyulassy, S.K. Kauffmann, and L.W. Wilson, *Phys. Rev. C* **20** (1979) 2267.
- [6] A. Fetter and J.D. Walecka, *Quantum Theory of Many-Particle Systems*, McGraw-Hill, New York (1971).
- [7] See I.V. Andreev, M. Plümer, and R.M. Weiner, *Int. J. Mod. Phys. A* **8** (1993) 4577, and references therein.
- [8] D.K. Srivastava and J.I. Kapusta, *Phys. Lett.* **B307** (1993) 1.
- [9] G. Baym and P. Braun-Munzinger, Los Alamos eprint archive nucl-th/9606055.

- [10] K. Kolehmainen and M. Gyulassy, Phys. Lett. B**180** (1986) 203.
- [11] S. Chapman and U. Heinz, Phys. Lett. B**340** (1994) 250.
- [12] E. Shuryak, Phys. Rev. B**44** (1973) 387; Sov. J. Nucl. Phys. **18** (1974) 667.
- [13] S. Pratt, Phys. Rev. Lett. **53** (1984) 1219; and Phys. Rev. D**33** (1986) 1314.
- [14] S. Chapman, P. Scotto, and U. Heinz, Heavy Ion Physics **1** (1995) 1.
- [15] J. Aichelin, Phys. Rep. **202** (1991) 233.
- [16] S. Padula, M. Gyulassy, and S. Gavin, Nucl. Phys. B**329** (1990) 357.
- [17] R. Hanbury Brown and R.Q. Twiss, Nature **178** (1956) 1046.
- [18] S. Chapman, J.R. Nix, and U. Heinz, Phys. Rev. C**52** (1995) 2694.
- [19] U.A. Wiedemann, P. Scotto and U. Heinz, Phys. Rev. C**53** (1996) 918.
- [20] S. Chapman, P. Scotto, and U. Heinz, Phys. Rev. Lett. **74** (1995) 4400.
- [21] S.V. Akkelin and Y.M. Sinyukov, Phys. Lett. B**356** (1995) 525.
- [22] T. Csörgő and B. Lörstad, Los Alamos eprint archive hep-ph/9509213; and Nucl. Phys. A**590** (1995) 465c.
- [23] U. Heinz, B. Tomášik, U.A. Wiedemann, and Y.-F. Wu, Phys. Lett. B**382** (1996) 181.
- [24] Y.-F. Wu, U. Heinz, B. Tomášik, and U.A. Wiedemann, Los Alamos eprint archive nucl-th/9607044, submitted to Phys. Rev. C.
- [25] A.N. Makhlin and Yu.M. Sinyukov, Z. Phys. C**39** (1988) 69.
- [26] G. Bertsch, Nucl. Phys. A**498** (1989) 173.
- [27] S. Pratt, T. Csörgő, and J. Zimányi, Phys. Rev. C**42** (1990) 2646.
- [28] M. Herrmann and G.F. Bertsch, Phys. Rev. C**51** (1995) 328.
- [29] B. Lörstad and T. Csörgő, in *Strangeness '96*, edited by T. Csörgő et al., Heavy Ion Physics (1996), in press.
- [30] B. Tomášik and U. Heinz, Regensburg preprint TPR-96-16, in preparation.
- [31] T. Csörgő and S. Pratt, in *Proceedings of the Workshop on Relativistic Heavy Ion Physics at Present and Future Accelerators*, Budapest, 1991, edited by T. Csörgő et al. (MTA KFKI Press, Budapest, 1991), p. 75.
- [32] D.H. Rischke and M. Gyulassy, Los Alamos eprint archive nucl-th/9606039, Nucl. Phys. A (1996), in press.
- [33] M.A. Lisa et al., Phys. Rev. Lett. **71** (1993) 2863.
- [34] M.A. Lisa et al., Phys. Rev. C**49** (1994) 2788.
- [35] NA35 Coll., T. Alber et al., Z. Phys. C**66** (1995) 77;  
NA35 Coll., T. Alber et al., Phys. Rev. Lett. **74** (1995) 1303.

- [36] NA44 Coll., H. Beker et al., Phys. Rev. Lett. **74** (1995) 3340.
- [37] K. Kadija for the NA49 Coll., in *Quark Matter '96*, (Heidelberg, 20.-24.5.1996), edited by P. Braun-Munzinger et al., Nucl. Phys. A, in press.
- [38] F. Yano and S. Koonin, Phys. Lett. **B78** (1978) 556.
- [39] M.I. Podgoretskiĭ , Sov. J. Nucl. Phys. **37** (1983) 272.
- [40] B.R. Schlei et. al., Phys. Lett. **B293** (1992) 275; J. Bolz et. al., Phys. Lett. **B300** (1993) 404; and Phys. Rev. **D47** (1993) 3860.
- [41] F. Cooper and G. Frye, Phys. Rev. **D10** (1974) 186.
- [42] A.N. Makhlin and Y.M. Sinyukov, Sov. J. Nucl. Phys. **46** (1987) 345.
- [43] S. Chapman and U. Heinz, unpublished notes (1994).
- [44] J. Aichelin, Los Alamos eprint archive nucl-th/9609006
- [45] J.D. Bjorken, Phys. Rev. **D27** (1983) 140.
- [46] U. Heinz, B. Tomášik, U.A. Wiedemann, and Y.-F. Wu, Los Alamos eprint archive nucl-th/9606041, Heavy Ion Physics (1996), in press.
- [47] S. Chapman and J.R. Nix, Los Alamos eprint archive nucl-th/9603007, Phys. Rev. C, in press.
- [48] NA49 Coll., T. Alber et al., Nucl. Phys. **A590** (1995) 453c; T. Alber, PhD thesis, MPI für Physik, München (1995), unpublished.
- [49] J. Sollfrank, P. Koch, and U. Heinz, Phys. Lett. **B252** (1990) 256; and Z. Phys. **C52** (1991) 593; E. Schnedermann, J. Sollfrank, and U. Heinz, Phys. Rev. **C48** (1993) 2462.
- [50] U.A. Wiedemann and U. Heinz, Regensburg preprint TPR-96-14, in preparation; U.A. Wiedemann, Invited lecture at the Triangle Meeting, School and Workshop on Heavy Ion Collisions, 1.-5. Sept. 1996, Bratislava, to appear in the Proceedings in Acta Phys. Slov.
- [51] U. Heinz, Los Alamos eprint archive nucl-th/9608002, in Ref. [ 4].
- [52] R. Hagedorn, Rivista Nuovo Cimento, vol. 6, serie 3, no. 10 (1983) 1.
- [53] F. Becattini, Z. Phys. **C69** (1996) 485, and private communication.
- [54] J. Letessier, A. Tounsi, U. Heinz, J. Sollfrank, J. Rafelski, Phys. Rev. **D51** (1995) 3408.
- [55] R. Hagedorn, *Relativistic Kinematics*, W.A. Benjamin, New York (1963).
- [56] P. Grassberger, Nucl. Phys. **B120** (1977) 231.
- [57] T. Csörgő, B. Lörstad, and J. Zimányi, Los Alamos eprint archive hep-ph/9411307, Z. Phys. C, in press.

**Keywords:** Two-particle interferometry / Hanbury-Brown-Twiss interferometry / HBT radii / relativistic heavy-ion collisions / quark-gluon plasma / resonance decays / collective flow / hydrodynamics / YKP parametrization / Mperp-scaling / emission function

**Abstract:** I discuss two-particle intensity interferometry as a method to extract from measured 1- and 2-particle momentum spectra information on the space-time geometry and dynamics of the particle emitting source. Particular attention is given to the rapid expansion and short lifetime of the sources created in relativistic heavy-ion collisions. Model-independent expressions for the HBT size parameters in terms of the space-time variances of the source are derived, and a new parametrization of the correlation function is suggested which allows to separate the transverse, longitudinal and temporal extension of the source and to measure its transverse and longitudinal expansion velocity. The effects of resonance decays are also discussed.